Analysis of the rotationally-resolved 3.3 μm region of C2H4 in natural isotopic abundance

O. Ben Fathallah, J. Vander Auwera, M. Tudorie, Vincent Boudon, Cyril Richard, M.A. Loroño-Gonzalez, Hassen Aroui, Maud Rotger

Analysis of the rotationally-resolved 3.3 μm region of C_2H_4 in natural isotopic abundance

O. BEN FATHALLAH [1,2], J. VANDER AUWERA[3], M. TUDORIE[3], V. BOUDON [4], C. RICHARD [4], M.A. LOROÑO GONZALEZ [5], H. AROUI [2], M. ROTGER[1]

[1]Université de Reims Champagne Ardenne, CNRS, GSMA UMR 7331, 51097 Reims, France.
[2]Université de Tunis, Ecole Nationale Supérieure d'Ingénieurs de Tunis, Laboratoire de Spectroscopie et dynamique Moléculaire, 1008 Tunis, Tunisie.
[3]SQUARES, C.P. 160/09, Université Libre de Bruxelles, 50 avenue F. D. Roosevelt, B-1050 Brussels, Belgium.
[4]Laboratoire ICB, UMR 6303 CNRS/Univ. Bourgogne, 9, av. Alain Savary, B.P. 47870, F-21078 Dijon, France.
[5]Oficina 410, Departamento Académico de Fisicoquímica,, Facultad de Química e Ingeniería Química, Universidad Nacional Mayor de San Marcos, Lima, Perú.

Abstract

Ethylene (or ethene) is a natural gas compound present in our atmosphere but also in the atmospheres of outer solar system planets such as Jupiter, Saturn, Uranus, Neptune and Saturn's moon Titan. However, a better knowledge of spectroscopic parameters is needed for this molecule in order to detect its presence and/or to derive its accurate concentration. We present here a detailed analysis and modeling of the strongly absorbing ν_9 and ν_{11} fundamental bands in the 3.3 μm region. Due to the complexity of the observed spectrum, we have built a polyad scheme taking into account some fundamental bands previously analyzed thanks to the tensorial formalism developed in Dijon for asymmetric-top molecules. A four polyad system has been settled and the last P_3 polyad contains five vibrational states: ν_9, ν_{11}, $\nu_2+\nu_{12}$ and $2\nu_{10}+\nu_{12}$. A first frequency analysis has been performed, leading to 3328 assignments with a root mean square of 5.927×10^{-3} cm^{-1} and a standard deviation of 1.965 using 88 adjusted parameters, and we have also adjusted line intensities of 2190 lines by adjusting 14 parameters with an overall Root-Mean-Square (RMS) deviation of about 3.77%. A new line list of calculated lines in the $2900-3300$ cm^{-1} region has been added to the ECaSDa and we plan to integrate it to the HITRAN database.

Keywords:
Ethylene, High-resolution infrared spectroscopy, Line positions, Tensorial formalism, Molecular spectroscopy database.

1. Introduction

Ethylene (or ethene, C_2H_4) is present in the atmosphere of various planetary bodies of the Solar system. On the Earth, it is a tropospheric compound of both natural and anthropogenic origins [1-4], characterized by a relatively short lifetime because of its reactivity with O_3 and OH [1]. C_2H_4 has also been observed in the atmosphere of outer Solar system objects, such as Jupiter [5], Saturn [6], Titan [7] and Neptune [8]. Detection of ethylene in these environments using optical remote sensing techniques rely on the strong *Q* branch structure of the ν_7 band near 10.5 μm [9].

The infrared spectrum of ethylene has been quite extensively studied (reviews of previous work until 2016 can be found in [10, 11]). These studies mainly focused on the strong 10 μm region, which corresponds to the excitation of 7 of the 12 modes of vibration of the molecule [10], of which 4 are infrared active [9]. The bands of this spectral region were also assigned by Ulenikov *et al.* [12, 13] while taking into account of different types of resonance interactions between bands. Likewise, other hot bands are studied in the 10 μm region such as $\nu_7+\nu_{10}-\nu_{10}$ and $\nu_{10}+\nu_{12}-\nu_{10}$ [14, 15].

At higher energies, the 1800 – 2400 cm^{-1} range, involving combination and overtone bands, was studied at high resolution, relying on conventional infrared or Raman spectroscopy ([16] and references therein) as well as jet cooled absorption spectra [17].

Of the 4 CH stretching modes of vibration of C_2H_4, only $\nu_9 = 1$ (near 3105 cm^{-1}) and $\nu_{11} = 1$ (near 2989 cm^{-1}) are infrared active. Several high-resolution studies were devoted to the corresponding absorption region, which roughly extends from 2900 to 3300 cm^{-1} [18-21], including measurements and analysis of line intensities [22]. The 3.3 μm energy range of $^{12}C_2H_4$ is particularly complex, as in particular demonstrated by the study of Sartakov *et al*. [19] that involved 34 vibrational levels to reproduce observed line positions. Variational calculations from ab initio potential energy and dipole moment surfaces were also reported [23].

Relying on high resolution Fourier transform spectra, the present work is an attempt to improve the analysis of the 3.3 μm spectral region of ethylene. To this end, we considered a polyad scheme composed of four polyads for the construction of the effective Hamiltonian model, namely: the ground-state (P_0), a dyad (P_1), a triad (P_2) and a tetrad (P_3) corresponding to the 3.3 μm region.

The article is organized as follows. Section 2 describes the recording of the high-resolution absorption spectra and measurements of $^{12}C_2H_4$ line positions and intensities. The theoretical model is described in Section 3. The analysis performed and results obtained are detailed in Section 4. Comparisons with previous work are also presented in this Section, before

concluding.

2. Experimental details

Three unapodized absorption spectra of ethylene (Praxair, 99.95 % stated purity) in natural isotopic abundance were recorded with a Bruker IFS 120 to 125HR upgrade Fourier transform spectrometer. The instrument was fitted with a tungsten source, a KBr beamsplitter, a low-pass (in wavenumber) optical filter with a cut-off wavenumber at about 5000 cm^{-1} and an InSb detector cooled down to 77 K. The sample was contained in a 19.7 ± 0.2 cm long stainless-steel cell installed in the evacuated spectrometer, closed by KBr windows and operated at room temperature (295 ± 1 K). The sample pressure was measured using a MKS Baratron gauge model 690A of 10 Torr full scale range, its accuracy of reading being conservatively estimated to be 0.5 %. The 3 spectra recorded correspond to sample pressures of 0.626 (3) hPa (spectrum S1), 1.201 (6) hPa (spectrum S2) and 2.568 (13) hPa (spectrum S3). They were recorded with a maximum optical difference (MOPD) of 150 cm, corresponding to an approximate spectral resolution (defined as 0.9/MOPD) of 0.006 cm^{-1}, using an entrance aperture diameter of 0.5 mm and result from the average of 360 to 400 interferograms. Transmittance spectra were generated using low resolution empty cell spectra recorded in-between the sample spectra. In the recorded spectral range (2900 to 3300 cm^{-1}), the strongest bands observed are ν_9, ν_{11}, $\nu_2 + \nu_{12}$ and $2\nu_{10} + \nu_{12}$ [10]. Weak bands, such as $\nu_3+\nu_8+\nu_{10}$ and $\nu_6+\nu_8+\nu_{10}$, are also present in this region [19]. It was shown [11] that about 50 bands (~ 90 % of them involving “dark states”) fall in this spectral range.

The positions of C_2H_4 lines as well as absorption lines of residual water vapor present in the evacuated spectrometer and observed in the range 3600 – 3880 cm^{-1} were measured with the program WSpectra [24]. Each line was modeled using a Gaussian or Voigt profile and the instrumental effects arising from the truncation of the interferogram and the finite diameter of the entrance aperture were included as fixed contributions. About 3600, 4000 and 6300 C_2H_4 line positions were thus measured in spectra S1 to S3. Comparison of the positions of the same lines measured in the 3 spectra showed that the precision of measurement is of the order of 0.0002 cm^{-1} for most of the lines. The measured positions $\tilde{\nu}_{obs}$ of 25 water vapor lines were matched to reference positions $\tilde{\nu}_{ref}$ available in HITRAN [25], originating from a linelist generated by Toth [26] and characterized by uncertainties ranging from 0.001 to 0.01 cm^{-1}. The differences $\tilde{\nu}_{ref} - \tilde{\nu}_{obs}$ were fitted to the expression $\tilde{\nu}_{ref} - \tilde{\nu}_{obs} = a\,\tilde{\nu}_{obs}$ (a was an adjusted

parameter), leading to an RMS deviation of 3.3×10^{-5} cm^{-1}. The ethylene spectra and line positions were calibrated using this expression and value of the parameter thus determined.

The intensities of the C_2H_4 lines were measured using the multi-spectrum fitting algorithm developed in Brussels ([27] and references therein). The program adjusts a synthetic spectrum to any number of observed spectra using a Levenberg Marquardt least squares fitting procedure. Each synthetic spectrum, calculated on a wavenumber grid interpolated 4 times with respect to the corresponding observed spectrum, is calculated as the convolution of the molecular transmittance spectrum with an instrument line shape (ILS) function. In the present work, the ILS included the effects of the finite MOPD and finite diameter of the entrance aperture of the interferometer as fixed contributions. The spectral baseline was represented by a fitted constant value. The profile of the lines was modeled using a Voigt function, with Gaussian width always fixed to the value calculated for Doppler broadening and the self-broadening coefficient of all the lines set to 0.125 cm^{-1}/atm [28]. The required initial values of the line parameters were generated using WSpectra, following the same procedure as for H_2O (see above). The measurements were performed based on the 3 spectra, however one spectrum at a time. Considering lines with peak transmittance up to 0.99, the intensities of 4153 lines were thus measured in one to three of the spectra S1 to S3. The line intensities measured in more than one spectrum were averaged.

Considering the uncertainties on the pressures, temperature and absorption path length as well as the precision of measurement of the line intensities provided by the least squares fitting procedure, we estimated that the overall uncertainties on line intensities are around 4% or better. Larger uncertainties characterize smaller line intensities. Dang-Nhu *et al.* [22] measured the intensities of 157 ethylene lines observed between 2966 and 3976 cm^{-1}. The uncertainties characterizing these line intensities are not provided in [22]. However, line intensities available in HITRAN [48] for the 3.3 um of C_2H_4, characterized by uncertainties ranging from 5 to 10 %, originate from [22]. Differences between 127 line intensities reported in [22] and measured in the present work are characterized by RMS deviations between 3.6 and 4.5 %.

3. Theoretical model

C_2H_4, is an asymmetric top molecule belonging to the D_{2h} symmetry point group. It possesses twelve normal modes of vibration [10]. In addition to the two active infrared fundamental bands ν_9 and ν_{11} with B_{3u} and B_{1u} symmetries centered at 3104.941 and 2988.653 cm^{-1}, respectively, the 3000 cm^{-1} studied region contains among numerous combination

bands and overtones [11]: two main combination bands, $\nu_2 + \nu_{12}$ and $2\nu_{10} + \nu_{12}$, centered at 3074.920 and 3100.040 cm^{-1}. This band system is strongly affected by resonances such as the Coriolis interactions and Fermi resonances.

As a matter of fact, from the positions of the band centers of ν_9 and ν_{11} bands, one can estimate that a close Coriolis resonance through rotation about the *c* axis, which is parallel to the C-C bond, can occur.

The upper states of ν_{11} exhibit a strong Fermi resonance with those of the $\nu_2 + \nu_{12}$ combination band.

The main interactions are of Coriolis type (see Figure 1). Moreover, the strong Fermi interaction between the $2\nu_{10}+\nu_{12}$, $\nu_2+\nu_{12}$ levels makes difficult to model of the tail of the *Q*-branch of the ν_9 band. Consequently, we are faced with two aspects that require improvements: the determination of both line intensities and line positions, which had been only partially performed before. It is also worth to mention that the $2\nu_{10} + \nu_{12}$ band can also strongly perturbate perpendicular type bands like ν_9. All theses interactions are summarized in the Fig. 1 below.

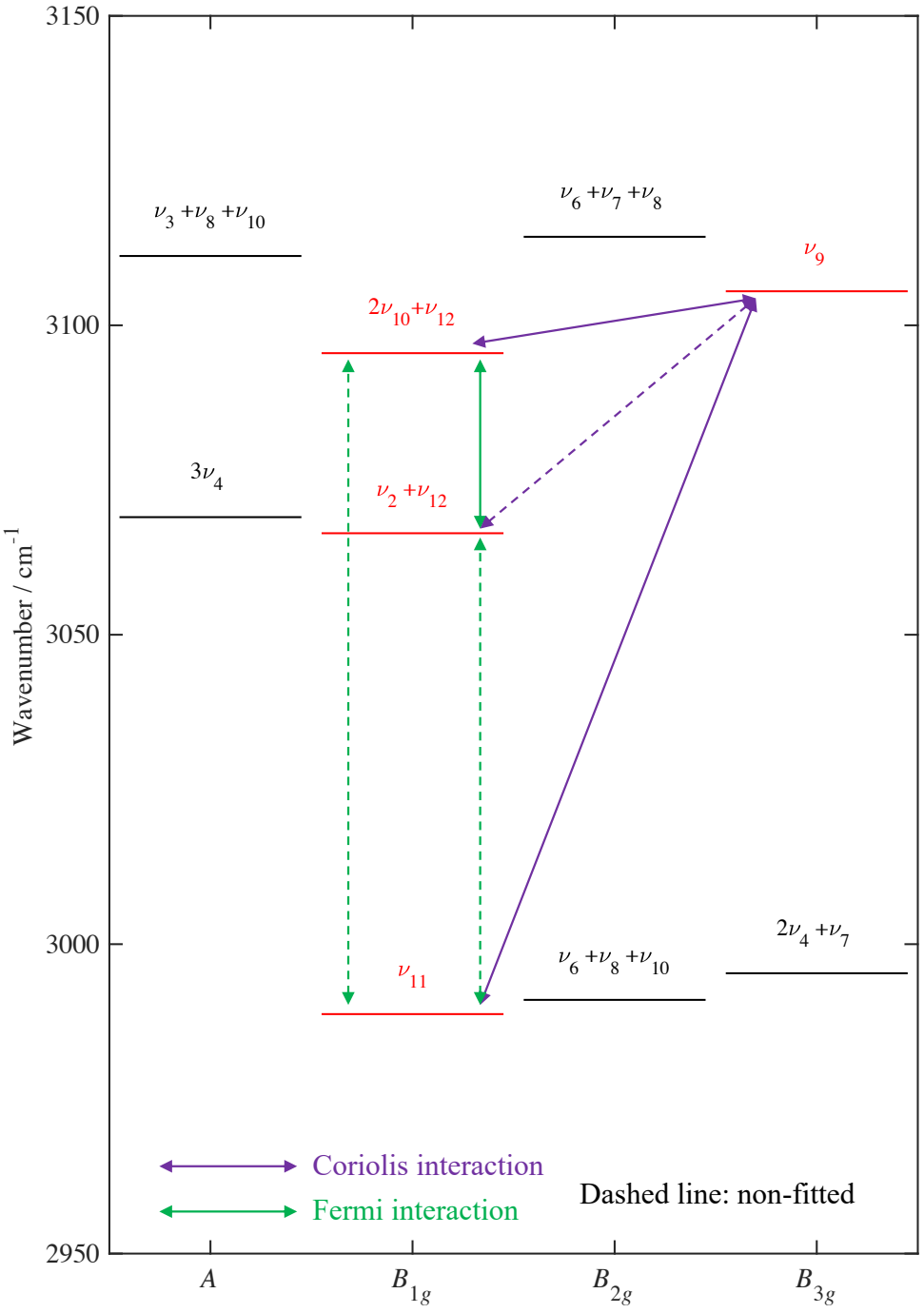

***Fig. 1**: The most important interactions between the levels $v_9 = 1$, $v_{11} = 1$, $v_2 + v_{12} = 1$ and $v_{10} + 2v_{12} = 1$ in the spectral region between 2900 and 3300 cm^{-1} of C_2H_4. Interactions represented by dashed lines could not be fitted in the present study.*

3.1. Effective Hamiltonian

In this paper, we use a theoretical model based on the tensorial formalism and the vibrational extrapolation concept developed by the Dijon group [29-31]. It takes full advantage of the molecule's high symmetry. Though the treatment of asymmetric-top molecules could be carried out without using irreducible tensor operators, their use allows a systematic and unified formulation of both effective [32] and exact nuclear-motion

Hamiltonians [11], at any order of the expansion and whatever the symmetry point group. In particular, the use of the tensor formalism turns out to be of primary importance when dealing with non-Abelian point groups [33]. Let us just recall briefly the basic principles of this model, which have been already detailed in Ref. [34]. Considering an X_2Y_4 molecule such as C_2H_4, the vibrational levels can be grouped in a series of polyads named P_k with $k = 0, ..., n$; the $P_{k=0}$ corresponds to the ground state (*GS*). The P_1 polyad is a dyad composed of the two vibrational bands: ν_{10} and ν_{12}. Then, the P_2 polyad is a triad including the ν_2, $\nu_{10} + \nu_{12}$ and $2\nu_{10}$ vibrational bands and the last P_3 polyad contains four bands: ν_9, ν_{11}, $\nu_2 + \nu_{12}$ and $2\nu_{10} + \nu_{12}$.

Assuming known the perturbative treatment using contact transformations method [34] in order to eliminate inter-polyad interactions, the Hamiltonian operator can be written as:

$$H = H_{\{P_0\}} + H_{\{P_1\}} + \ldots + H_{\{P_k\}} + \ldots + H_{\{P_{n-1}\}} + H_{\{P_n\}}. \quad (1)$$

The different $H_{\{P_k\}}$ terms are expressed in the following form:

$$H_{\{P_k\}} = \sum_{all\ indexes} \beta t^{\Omega(K,n\Gamma)\Gamma_v\Gamma'_v}_{\{s\}\{s'\}} \left[{}^{\varepsilon}V^{\Omega_v(\Gamma_v\Gamma'_v)\Gamma}_{\{s\}\{s'\}} \otimes R^{\Omega(K,n\Gamma)} \right](A_1). \quad (2)$$

In this equation, the $t^{\Omega(K,n\Gamma)\Gamma_v\Gamma'_v}_{\{s\}\{s'\}}$ are the parameters to be determined by data fitting while ${}^{\varepsilon}V^{\Omega_v(\Gamma_v\Gamma'_v)\Gamma}_{\{s\}\{s'\}}$ and $R^{\Omega(K,n\Gamma)}$ are the vibrational and rotational operators, respectively. For each term, Ω_v and Ω represent the degree in elementary vibrational operators (creation a^+ and annihilation a operators), and rotational operators (components J_x, J_y and J_z of the angular momentum), respectively. β is a numerical factor equal to:

$$\beta = \begin{cases} \left(-\frac{\sqrt{3}}{4}\right)^{\frac{\Omega}{2}} & if\ (K, n\Gamma_r) = (0, 0A_g) \\ 1 & if\ (K, n\Gamma_r) \neq (0, 0A_g) \end{cases}. \quad (3)$$

The order of each individual term is defined as $\Omega + \Omega_v - 2$. We deal with the effective Hamiltonians which are obtained, for a given polyad P_k, by the projection of H on the P_n Hilbert subspace:

$$\tilde{H}^{\langle Pn\rangle} = P^{\langle Pn\rangle}\ H\ P^{\langle Pn\rangle} = H^{\langle P_n\rangle}_{\{GS\}} + H^{\langle P_n\rangle}_{\{P_1\}} + ... + H^{\langle P_n\rangle}_{\{P_k\}} + ... + H^{\langle P_n\rangle}_{\{P_{n-1}\}} + H^{\langle P_n\rangle}_{\{P_n\}}. \quad (4)$$

In the case of ethylene, which exhibits an unclear polyad structure beyond 1200 cm^{-1} contrary to other molecules like methane, for the present study, we have defined the following effective Hamiltonians:

- The ground state effective Hamiltonian,

$$\tilde{H}^{\langle GS\rangle} = H^{\langle GS\rangle}_{\{GS\}}. \quad (5)$$

- The ν_{10}/ν_{12} dyad effective Hamiltonian,

$$\tilde{H}^{\langle \nu_{10}/\nu_{12}\rangle} = H^{\langle \nu_{10}/\nu_{12}\rangle}_{\{GS\}} + H^{\langle \nu_{10}/\nu_{12}\rangle}_{\{\nu_{10}/\nu_{12}\}}. \quad (6)$$

- The triad $\nu_2/\nu_{10} + \nu_{12}/2\ \nu_{10}$ effective Hamiltonian,

$$\tilde{H}^{\langle Triad\rangle} = H^{\langle Triad\rangle}_{\{GS\}} + H^{\langle Triad\rangle}_{\{Triad\}} = H^{\langle \nu_2/\nu_{10}+\nu_{12}/2\nu_{10}\rangle}_{\{GS\}} + H^{\langle \nu_2/\nu_{10}+\nu_{12}/2\nu_{10}\rangle}_{\{\nu_2\}} + H^{\langle \nu_2/\nu_{10}+\nu_{12}/2\nu_{10}\rangle}_{\{\nu_{10}+\nu_{12}\}} + H^{\langle \nu_2/\nu_{10}+\nu_{12}/2\nu_{10}\rangle}_{\{2\nu_{10}\}} \quad (7)$$

- The tetrad $\nu_9/\ \nu_{11}/2\nu_{10} + \nu_{12}/\ \nu_2 + \nu_{12}\ /$ effective Hamiltonian,

$$\tilde{H}^{\langle Tetrad\rangle} = H^{\langle Tetrad\rangle}_{\{GS\}} + H^{\langle Tetrad\rangle}_{\{Tetrad\}} = H^{\langle \nu_9/\nu_{11}/\nu_2+\nu_{12}/2\nu_{10}+\nu_{12}\rangle}_{\{GS\}} + H^{\langle \nu_9/\nu_{11}/\nu_2+\nu_{12}/2\nu_{10}+\nu_{12}\rangle}_{\{\nu_9\}} + H^{\langle \nu_9/\nu_{11}/\nu_2+\nu_{12}/2\nu_{10}+\nu_{12}\rangle}_{\{\nu_{11}\}} + H^{\langle \nu_9/\nu_{11}/\nu_2+\nu_{12}/2\nu_{10}+\nu_{12}\rangle}_{\{\nu_2+\nu_{12}\}} + H^{\langle \nu_9/\nu_{11}/\nu_2+\nu_{12}/2\nu_{10}+\nu_{12}\rangle}_{\{2\nu_{10}+\nu_{12}\}}. \quad (8)$$

3.2. Effective dipole moment

In order to calculate transition absolute intensities, we also need to expand the effective dipole moment operator using a coupling scheme similar to that of the Hamiltonian [34]. The dipole moment being a vector quantity, we have to determine how the three components *x, y* and *z* will transform in D_{2h}. In this work, only the parameters for the four cold band transitions corresponding to ν_9, ν_{11}, $\nu_2+\nu_{12}$ and $2\nu_{10}+\nu_{12}$ have been adjusted.

3.3. Basis sets and line intensities

The calculation of the effective Hamiltonian and effective dipole moment matrix elements are performed in the coupled rovibrational basis, $\left|\left[\psi_v^{(C_v,C_v)} \otimes \psi_r^{(J,C_r,C_r)}\right]^{(C)}\right\rangle$, where

$\psi_r^{(J,C_r,C_r)}$ is a rotational wavefunction with angular momentum *J* and rotational symmetry species C_r in *D2h* symmetry group, $\psi_v^{(C_v,C_v)}$ is a coupled vibrational basis set; and C is the overall symmetry species ($C = C_v \otimes C_r$). In the present case, $\psi_v^{(C_v,C_v)}$ contains the relevant functions for the vibrational normal modes of the tetrad,

$$\left|\psi_v^{(C_v,C_v)}\right\rangle = \left|\psi_{\sigma_v}^{(v,l,C_v,C_v)}\right\rangle. \quad (9)$$

The effective Hamiltonian matrix is diagonalized numerically, and this leads to eigenfunctions obtained from,

$$\tilde{H}\left|\psi_\sigma^{(J,C,C\alpha)}\right\rangle = E\left|\psi_\sigma^{(J,C,C_v\alpha)}\right\rangle, \quad (10)$$

where $\alpha = 1, 2, \ldots$ is a counting number to distinguish functions with the same symmetry C in a given *J* block. This eigenbasis set can be expanded in terms of the initial rovibrational basis set and is used to calculate the matrix elements of the effective dipole moment operator $\tilde{\mu}$.

The line intensity at temperature *T* for a transition at wavenumber $\tilde{\nu}_{if}$, between an initial state *i* (with energy E_i) and a final state *f*, is then obtained through:

$$S_{if}(cm^{-1}/(molecule.cm^{-2})) = \frac{8\Pi^3}{hcQ}\tilde{\nu}_{if}e^{-\frac{E_i}{k_BT}}\left(1-e^{-\frac{hc\tilde{\nu}_{if}}{k_BT}}\right)\left|\sum_{\alpha_i,\alpha_f}\left\langle\psi_{\sigma_f}^{(J_i,C_i,C_i\alpha_i)}\left|\mu_Z\right|\psi_{\sigma_f}^{(J_f,C_f,C_f\alpha_f)}\right\rangle\right|^2. \quad (11)$$

Q is the total partition function at temperature *T* (calculated thanks to a simple harmonic approximation for vibration [35] and the rotational approximation for asymmetric top molecules given in Ref. [36]), *c* is the speed of light in vacuum, *h* the Planck's constant and k_B the Boltzmann's constant.

4. Analysis and discussion

4.1. Line positions for the tetrad

The XTDS [37] computational package has been used to generate the Hamiltonian and dipole moment model as well as to fit the effective parameters to the observed data. As previously mentioned, the 3000 cm^{-1} region of C_2H_4 includes the ν_9, ν_{11}, $2\nu_{10}+\nu_{12}$

and $\nu_2 + \nu_{12}$ bands and exhibits complex spectral rovibrational patterns due to many resonance couplings that may lead to intensity exchanges between weak and strong lines. The presence of so-called dark states that are not observed may also strongly affect the adjustment of the effective parameters and thus locally affect accuracy of both line positions and line intensities. For example, the combination bands $v_3 + v_8 + v_{10}$ and $v_6 + v_8 + v_{10}$ have very low intensities and were not taken into account in our polyad scheme [19]. Using the predictions in Ref. [11], we can estimate that the intensities for these bands are about 80 and 800 times smaller than those of the v_9 band. Also, the $v_6 + v_7 + v_8$ band is not taken into account in the band scheme because it has an intensity 33 times smaller.

Note that Lebron *et al.* [38] studied each band separately using the Watson's asymmetric top Hamiltonian in the standard A-reduced form and the I^r representation. This reproduced the undisturbed lines, which would later be used in the tensorial formalism. Using the D_{2h}TDS package combined with the graphical SPVIEW environment [37, 39], each unperturbed line was identified for each band separately. Likewise, the v_{11} band also presents a Coriolis interaction with the v_9 band. In order to account for strong interactions, we have also explicitly introduced resonance parameters between $v_2 + v_{12}$ and v_{11} in the model. Such an interaction is supposed to be very strong according to Refs. [40, 41]. By considering this Fermi interaction, we were able to model the overall Q branch of the v_{11} band.

The assignment procedure was rather straightforward. Initial parameters for the ground state, v_2[42], v_{12}, v_{10} and $2v_{10}$ [43] were taken from literature. For the v_9, v_{11} and $v_2 + v_{12}$ bands, we have converted the Watson's parameters [38, 44] to the tensorial ones as explained in the appendix. As a starting point, we have considered few hundreds of assigned lines up to $J = 5$ deduced from the variational calculation [11]. This allowed to generate quite easily a new set of parameters using a least-squares fitting as well as a new prediction file that was used for further assignments. This process was repeated until assigning 1810 lines of the v_9 band, 1307 of v_{11}, 143 of $v_2 + v_{12}$ and 68 of $2v_{10} + v_{12}$.

The final fit involves an effective Hamiltonian developed up to the eighth order that allowed obtaining an overall RMS deviation of 5.927×10^{-3} cm^{-1} and a standard deviation of 1.965. Table 1 gives the list of tensorial rovibrational parameters (in cm^{-1}) obtained from these fits. Table 2 summarizes the statistics for the final fit of the studied spectral region.

For the $2v_{10} + v_{12}$ band, the corresponding Watson's parameters are absent in the literature, so they have been calculated by formula in the sub-section 4.2 and summarized in Table 2 with those of the other bands. We can note that the rovibrational parameters derived

from this fit are in good agreement with those from previous works [38, 44].

Table 1: Effective Hamiltonian parameters for the GS, ν_9, ν_{11}, $\nu_2 + \nu_{12}$ and $2\nu_{10} + \nu_{12}$ bands of C_2H_4 and comparison with Ref. [21].

Levels	Order	Vibrational States			Values / cm^{-1}	Values of Ref. [21] / cm^{-1}
		$\Omega(K,n\Gamma)$	Γ_v	Γ'_v		
$\nu_9 = 1$						
	0	$0(0,0A_g)$	$000000001000B_{3u}$	$000000001000B_{3u}$	3104.88580(33)	3104.87443(17)
	2	$2(0,0A_g)$	$000000001000B_{3u}$	$000000001000B_{3u}$	$-7.461(12)\times10^{-03}$	$-6.451(13)\times10^{-03}$
		$2(2,0A_g)$	$000000001000B_{3u}$	$000000001000B_{3u}$	$-3.2683(49)\times10^{-03}$	$-2.4808(60)\times10^{-03}$
		$2(2,1A_g)$	$000000001000B_{3u}$	$000000001000B_{3u}$	$-7.99(42)\times10^{-05}$	$1.1469(29)\times10^{-03}$
	4	$4(0,0A_g)$	$000000001000B_{3u}$	$000000001000B_{3u}$	$-1.153(11)\times10^{-05}$	$-5.363(34)\times10^{-05}$
		$4(2,0A_g)$	$000000001000B_{3u}$	$000000001000B_{3u}$	$4.201(39)\times10^{-06}$	$2.9860(95)\times10^{-05}$
		$4(2,1A_g)$	$000000001000B_{3u}$	$000000001000B_{3u}$	$1.227(20)\times10^{-05}$	$2.1063(92)\times10^{-04}$
		$4(4,0A_g)$	$000000001000B_{3u}$	$000000001000B_{3u}$	$-2.130(18)\times10^{-06}$	$-2.343(27)\times10^{-06}$
		$4(4,1A_g)$	$000000001000B_{3u}$	$000000001000B_{3u}$	$-1.827(30)\times10^{-05}$	$-3.2306(14)\times10^{-04}$
		$4(4,2A_g)$	$000000001000B_{3u}$	$000000001000B_{3u}$	$7.829(90)\times10^{-07}$	-1.085×10^{-05}
	6	$6(0,0A_g)$	$000000001000B_{3u}$	$000000001000B_{3u}$	$4.037(58)\times10^{-08}$	$5.071(28)\times10^{-07}$
		$6(2,0A_g)$	$000000001000B_{3u}$	$000000001000B_{3u}$	$7.19(11)\times10^{-09}$	$4.428(46)\times10^{-08}$
		$6(2,1A_g)$	$000000001000B_{3u}$	$000000001000B_{3u}$	$2.939(20)\times10^{-08}$	$2.036(12)\times10^{-08}$
		$6(4,0A_g)$	$000000001000B_{3u}$	$000000001000B_{3u}$	$-5.098(74)\times10^{-09}$	$-6.659(20)\times10^{-08}$
		$6(4,1A_g)$	$000000001000B_{3u}$	$000000001000B_{3u}$	$-7.245(30)\times10^{-08}$	$-4.958(25)\times10^{-08}$
		$6(4,2A_g)$	$000000001000B_{3u}$	$000000001000B_{3u}$	$-1.19(23)\times10^{-09}$	$-6.483(36)\times10^{-09}$
		$6(6,0A_g)$	$000000001000B_{3u}$	$000000001000B_{3u}$	$2.530(18)\times10^{-09}$	$1.03858(63)\times10^{-07}$
		$6(6,1A_g)$	$000000001000B_{3u}$	$000000001000B_{3u}$	$3.652(14)\times10^{-08}$	$2.264(10)\times10^{-08}$
		$6(6,2A_g)$	$000000001000B_{3u}$	$000000001000B_{3u}$	$2.01(36)\times10^{-09}$	$-1.958(54)\times10^{-09}$
		$6(6,3A_g)$	$000000001000B_{3u}$	$000000001000B_{3u}$	$-2.706(80)\times10^{-10}$	$3.07(47)\times10^{-11}$
	8	$8(0,0A_g)$	$000000001000B_{3u}$	$000000001000B_{3u}$	$-6.63(11)\times10^{-11}$	
		$8(2,0A_g)$	$000000001000B_{3u}$	$000000001000B_{3u}$	$4.64(14)\times10^{-12}$	
		$8(2,1A_g)$	$000000001000B_{3u}$	$000000001000B_{3u}$	$2.2918(66)\times10^{-11}$	
		$8(4,0A_g)$	$000000001000B_{3u}$	$000000001000B_{3u}$	$-4.474(85)\times10^{-12}$	
		$8(4,1A_g)$	$000000001000B_{3u}$	$000000001000B_{3u}$	$-7.269(12)\times10^{-11}$	
		$8(4,2A_g)$	$000000001000B_{3u}$	$000000001000B_{3u}$	$3.47(57)\times10^{-13}$	
		$8(6,0A_g)$	$000000001000B_{3u}$	$000000001000B_{3u}$	$3.060(41)\times10^{-12}$	
		$8(6,1A_g)$	$000000001000B_{3u}$	$000000001000B_{3u}$	$6.455(59)\times10^{-11}$	
		$8(6,2A_g)$	$000000001000B_{3u}$	$000000001000B_{3u}$	$-8.45(89)\times10^{-13}$	
		$8(6,3A_g)$	$000000001000B_{3u}$	$000000001000B_{3u}$	$-1.689(22)\times10^{-13}$	
		$8(8,0A_g)$	$000000001000B_{3u}$	$000000001000B_{3u}$	$-1.351(10)^{*}\times10^{-12}$	
		$8(8,1A_g)$	$000000001000B_{3u}$	$000000001000B_{3u}$	$-1.9621(16)\times10^{-11}$	
		$8(8,2A_g)$	$000000001000B_{3u}$	$000000001000B_{3u}$	0.00	
		$8(8,3A_g)$	$000000001000B_{3u}$	$000000001000B_{3u}$	0.00	
		$8(8,4A_g)$	$000000001000B_{3u}$	$000000001000B_{3u}$	0.00	
$\nu_{11} = 1$						
	0	$0(0,0A_g)$	$000000000010B_{1u}$	$000000000010B_{1u}$	2988.6435(32)	2988.63465(16)
	2	$2(0,0A_g)$	$000000000010B_{1u}$	$000000000010B_{1u}$	$-3.3771(73)\times10^{-03}$	$-3.1248(57)\times10^{-03}$
		$2(2,0A_g)$	$000000000010B_{1u}$	$000000000010B_{1u}$	$-1.2597(34)\times10^{-03}$	$-1.2727(26)\times10^{-03}$
		$2(2,1A_g)$	$000000000010B_{1u}$	$000000000010B_{1u}$	$5.935(40)\times10^{-04}$	$-6.148(33)\times10^{-04}$
	4	$4(0,0A_g)$	$000000000010B_{1u}$	$000000000010B_{1u}$	$-6.053(40)\times10^{-06}$	$-8.649(49)\times10^{-06}$
		$4(2,0A_g)$	$000000000010B_{1u}$	$000000000010B_{1u}$	$1.974(36)\times10^{-06}$	$1.914(19)\times10^{-06}$
		$4(2,1A_g)$	$000000000010B_{1u}$	$000000000010B_{1u}$	$7.85(82)\times10^{-06}$	$-2.948(77)\times10^{-06}$
		$4(4,0A_g)$	$000000000010B_{1u}$	$000000000010B_{1u}$	$-1.210(32)\times10^{-06}$	$-1.095(15)\times10^{-06}$
		$4(4,1A_g)$	$000000000010B_{1u}$	$000000000010B_{1u}$	$-1.20(13)\times10^{-05}$	$4.55(11)\times10^{-06}$
		$4(4,2A_g)$	$000000000010B_{1u}$	$000000000010B_{1u}$	$3.46(37)\times10^{-07}$	0.00
	6	$6(0,0A_g)$	$000000000010B_{1u}$	$000000000010B_{1u}$	$3.766(83)\times10^{-09}$	0.00
		$6(2,0A_g)$	$000000000010B_{1u}$	$000000000010B_{1u}$	$6.07(27)\times10^{-10}$	0.00
		$6(2,1A_g)$	$000000000010B_{1u}$	$000000000010B_{1u}$	$-4.57(53)\times10^{-10}$	$9.6906(36)\times10^{-08}$

		6(4,0A_g)	000000000010B_{1u}	000000000010B_{1u}	-4.04(10) $\times 10^{-10}$	5.236(24) $\times 10^{-09}$
		6(4,1A_g)	000000000010B_{1u}	000000000010B_{1u}	0.85(11) $\times 10^{-10}$	-1.48639(52) $\times 10^{-07}$
		6(4,2A_g)	000000000010B_{1u}	000000000010B_{1u}	-2.16(30) $\times 10^{-10}$	-4.759(12) $\times 10^{-09}$
		6(6,0A_g)	000000000010B_{1u}	000000000010B_{1u}	2.39(28) $\times 10^{-10}$	1.140(34) $\times 10^{-09}$
		6(6,1A_g)	000000000010B_{1u}	000000000010B_{1u}	-1.98(44) $\times 10^{-10}$	-4.86(20) $\times 10^{-10}$
		6(6,2A_g)	000000000010B_{1u}	000000000010B_{1u}	3.22(49) $\times 10^{-10}$	3.94(18) $\times 10^{-10}$
		6(6,3A_g)	000000000010B_{1u}	000000000010B_{1u}	0.00	4.00(31) $\times 10^{-11}$
	8	8(0,0A_g)	000000000010B_{1u}	000000000010B_{1u}	0.00	
		8(2,0A_g)	000000000010B_{1u}	000000000010B_{1u}	0.00	
		8(2,1A_g)	000000000010B_{1u}	000000000010B_{1u}	0.00	
		8(4,0A_g)	000000000010B_{1u}	000000000010B_{1u}	0.00	
		8(4,1A_g)	000000000010B_{1u}	000000000010B_{1u}	0.00	
		8(4,2A_g)	000000000010B_{1u}	000000000010B_{1u}	0.00	
		8(6,0A_g)	000000000010B_{1u}	000000000010B_{1u}	0.00	
		8(6,1A_g)	000000000010B_{1u}	000000000010B_{1u}	0.00	
		8(6,2A_g)	000000000010B_{1u}	000000000010B_{1u}	0.00	
		8(6,3A_g)	000000000010B_{1u}	000000000010B_{1u}	0.00	
		8(8,0A_g)	000000000010B_{1u}	000000000010B_{1u}	0.00	
		8(8,1A_g)	000000000010B_{1u}	000000000010B_{1u}	0.00	
		8(8,2A_g)	000000000010B_{1u}	000000000010B_{1u}	0.00	
		8(8,3A_g)	000000000010B_{1u}	000000000010B_{1u}	0.00	
		8(8,4A_g)	000000000010B_{1u}	000000000010B_{1u}	0.00	
v_2=v_{12}=1						
	0	0(0,0A_g)	010000000001B_{1u}	010000000001B_{1u}	1.4078(12) $\times 10^{+01}$	
	2	2(0,0A_g)	010000000001B_{1u}	010000000001B_{1u}	8.34(15) $\times 10^{-03}$	
		2(2,0A_g)	010000000001B_{1u}	010000000001B_{1u}	4.361(77) $\times 10^{-03}$	
		2(2,1A_g)	010000000001B_{1u}	010000000001B_{1u}	1.777(12) $\times 10^{-03}$	
	4	4(0,0A_g)	010000000001B_{1u}	010000000001B_{1u}	-1.1414(62) $\times 10^{-04}$	
		4(2,0A_g)	010000000001B_{1u}	010000000001B_{1u}	5.919 (22) $\times 10^{-05}$	
		4(2,1A_g)	010000000001B_{1u}	010000000001B_{1u}	-1.2354(12) $\times 10^{-04}$	
		4(4,0A_g)	010000000001B_{1u}	010000000001B_{1u}	-3.1656(88) $\times 10^{-05}$	
		4(4,1A_g)	010000000001B_{1u}	010000000001B_{1u}	1.7199(19) $\times 10^{-04}$	
		4(4,2A_g)	010000000001B_{1u}	010000000001B_{1u}	-3.0636(99) $\times 10^{-06}$	
	6	6(0,0A_g)	010000000001B_{1u}	010000000001B_{1u}	-2.257(12) $\times 10^{-07}$	
		6(2,0A_g)	010000000001B_{1u}	010000000001B_{1u}	1.081(27) $\times 10^{-08}$	
		6(2,1A_g)	010000000001B_{1u}	010000000001B_{1u}	-1.15076(74) $\times 10^{-07}$	
		6(4,0A_g)	010000000001B_{1u}	010000000001B_{1u}	-5.903 (22) $\times 10^{-08}$	
		6(4,1A_g)	010000000001B_{1u}	010000000001B_{1u}	1.5847 (12) $\times 10^{-07}$	
		6(4,2A_g)	010000000001B_{1u}	010000000001B_{1u}	-2.7171(80) $\times 10^{-09}$	
		6(6,0A_g)	010000000001B_{1u}	010000000001B_{1u}	1.2287(62) $\times 10^{-08}$	
		6(6,1A_g)	010000000001B_{1u}	010000000001B_{1u}	0.00	
		6(6,2A_g)	010000000001B_{1u}	010000000001B_{1u}	0.00	
		6(6,3A_g)	010000000001B_{1u}	010000000001B_{1u}	0.00	
v_{10}=2,v_{12}=1						
	0	0(0,0A_g)	000000000201B_{1u}	000000000201B_{1u}	-6.344(13) $\times 10^{+00}$	
	2	2(0,0A_g)	000000000201B_{1u}	000000000201B_{1u}	1.754(13) $\times 10^{-02}$	
		2(2,0A_g)	000000000201B_{1u}	000000000201B_{1u}	8.181(60) $\times 10^{-03}$	
		2(2,1A_g)	000000000201B_{1u}	000000000201B_{1u}	-3.8765(65) $\times 10^{-03}$	
	4	4(0,0A_g)	000000000201B_{1u}	000000000201B_{1u}	4.998(23) $\times 10^{-05}$	
		4(2,0A_g)	000000000201B_{1u}	000000000201B_{1u}	10(5) $\times 10^{-08}$	
		4(2,1A_g)	000000000201B_{1u}	000000000201B_{1u}	-3.11 (56) $\times 10^{-08}$	
		4(4,0A_g)	000000000201B_{1u}	000000000201B_{1u}	0.00	
		4(4,1A_g)	000000000201B_{1u}	000000000201B_{1u}	0.00	
		4(4,2A_g)	000000000201B_{1u}	000000000201B_{1u}	0.00	
v_9=1 / v_{11}=1 interaction						
		1(1,0 B_{2g})	000000001000B_{3u}	000000000010B_{1u}	-1.86(83) $\times 10^{-02}$	
v_9=1 / v_{10}=2, v_{12}=1 interaction						

	1	1(1,0B_{2g})	000000001000B_{3u}	000000000201B_{1u}	5.554(88) ×10^{-03}
	2	2(2,0B_{2g})	000000001000B_{3u}	000000000201B_{1u}	3.815(34) ×10^{-03}
	3	3(1,0B_{2g})	000000001000B_{3u}	000000000201B_{1u}	-1.91(18) ×10^{-05}
		3(3,0B_{2g})	000000001000B_{3u}	000000000201B_{1u}	3.49(29) ×10^{-05}
		3(3,1B_{2g})	000000001000B_{3u}	000000000201B_{1u}	9.65(23) ×10^{-06}
	4	4(2,0B_{2g})	000000001000B_{3u}	000000000201B_{1u}	8.65(23) ×10^{-07}
		4(4,0B_{2g})	000000001000B_{3u}	000000000201B_{1u}	-6.42(16) ×10^{-06}
		4(4,1B_{2g})	000000001000B_{3u}	000000000201B_{1u}	-9(6) ×10^{-08}
	5	(1,0B_{2g})	000000001000B_{3u}	0000000000201B_{1u}	-3.02(59) ×10^{-09}
v_2=1, v_{12}=1 / v_{10}=2, v_{12}=1 interaction					
		0(0,0A_g)	010000000001B_{1u}	000000000201B_{1u}	9.595(11) ×10^{+00}
		2(0,0A_g)	010000000001B_{1u}	000000000201B_{1u}	-7.571(99) ×10^{-03}
		2(2,0A_g)	010000000001B_{1u}	000000000201B_{1u}	-8.20(51) ×10^{-04}
		2(2,1A_g)	010000000001B_{1u}	000000000201B_{1u}	0.00

Fig. 2 displays the experimental and calculated spectra in the region between 2900 and 3300 cm^{-1}, with the corresponding residuals.

In Fig. 3, we present the experimental and calculated spectra of the ν_{11} band, showing a good agreement between the observed and calculated line positions using the tensorial formalism. This agreement is illustrated by a low residual (Obs.-Calc.) in all branches of the ν_{11} band with an average difference of 1.96×10^{-3} cm^{-1}.

Fig. 4 shows the spectral region of the highly mixed ν_9 band with the two $\nu_2 + \nu_{12}$ and $2\nu_{10} + \nu_{12}$ combination bands. Here, the agreement between the observed and calculated positions is also good, resulting in a higher residual amplitude of approximatively 4.37×10^{-3} cm^{-1}.

Fig. 5 shows the simulation of the spectral region of the $\nu_2 + \nu_{12}$ and $2\nu_{10} + \nu_{12}$ bands. For 143 attributions of the $\nu_2 + \nu_{12}$ band and 68 attributions of the $2\nu_{10} + \nu_{12}$ band, a mean deviation of 3.80×10^{-3} and 4.82×10^{-3} cm^{-1} respectively was illustrated.

Table 1 compares our parameters with those reported by Loroño *et al*. [21], showing a notable discrepancy with our results. The authors of this reference investigated a much broader spectral range from 3000 to 6000 cm^{-1} and in our region of interest at 3.3 μm, they used a simplified polyad scheme where they take into account only the ν_9 and ν_{11} bands. It is worth noting that these obtained a remarkable level of accuracy in their study, assigning 682 transitions up to J_{max} = 32 while fitting 40 parameters of the Hamiltonian model with an RMS of 0.01 cm^{-1}.

Regarding the results, for the ν_9 and the ν_{11} bands, our analysis shows that 16 out of 20 parameters of ν_9 and 9 out of 15 parameters of the ν_{11} band are consistent, with identical signs, with those of Ref. [21].

Table 2: Statistics of the fit of the 3.3 μm region of the ethylene molecule.

Development order	8
Number of assignments	3328
Fitted parameters	88/606
Fixed parameters	79/606
Fixed parameters to 0	439/606
J_{max}	40
RMS deviation	5.927×10^{-3} cm^{-1}

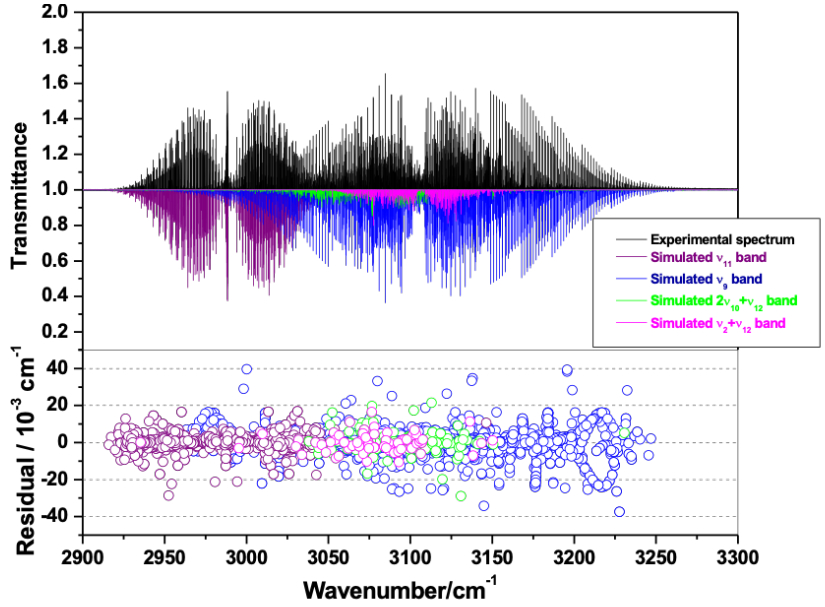

***Fig. 2**: Experimental and simulated spectrum of C_2H_4 in the region between 2900 and 3300 cm^{-1}; the bottom panel shows the residual for line positions (Obs-calc) for the assigned lines versus the experimental positions.*

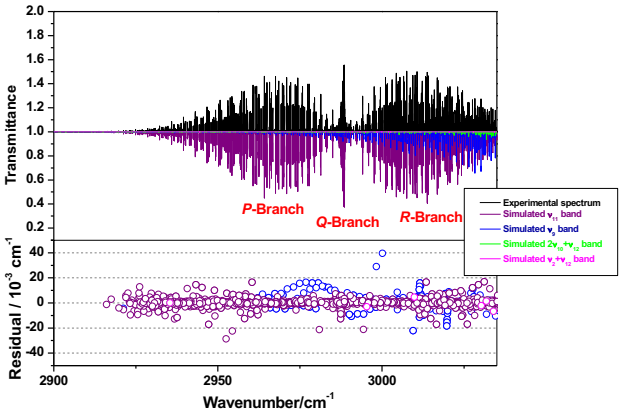

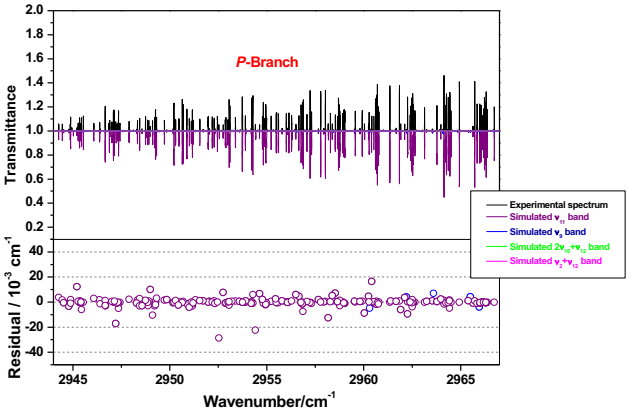

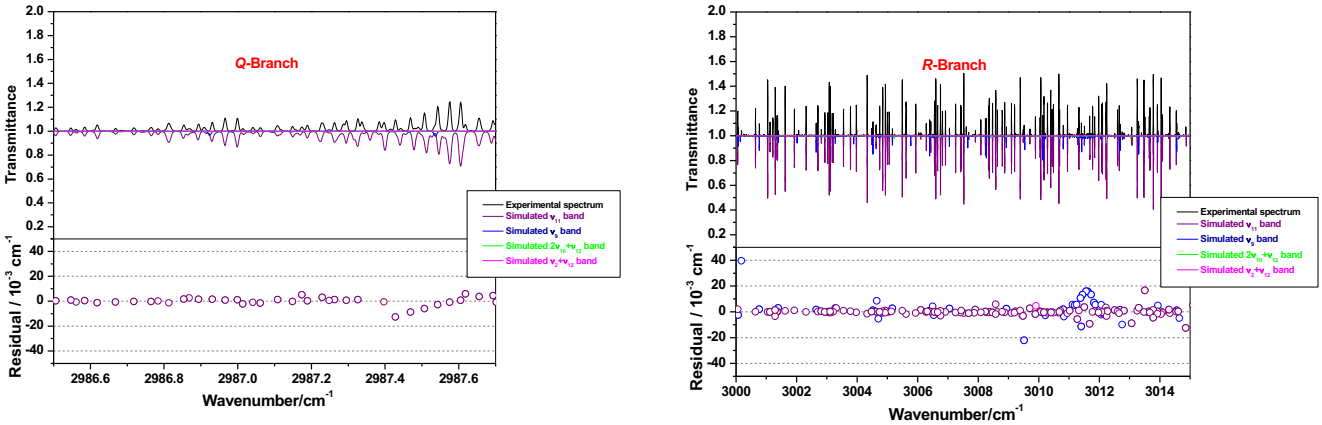

Fig. 3: Experimental and simulated C_2H_4 spectrum of the ν_{11} band. The lower panels show the residuals for line positions in each part of the spectrum versus the experimental positions.

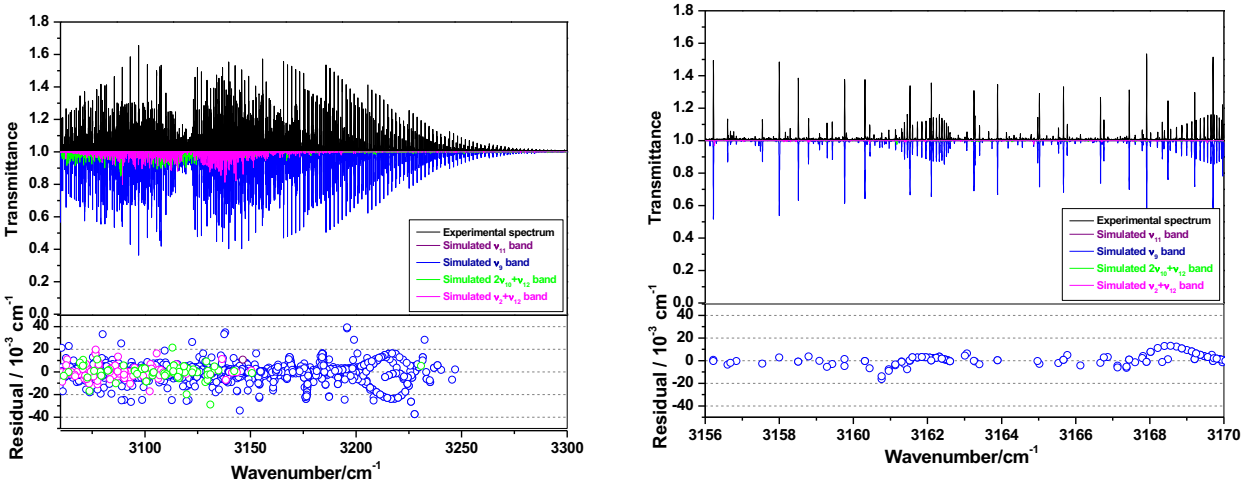

Fig. 4: Experimental and simulated spectrum of C_2H_4 in the spectral region between 3060 and 3300 cm^{-1}. The lower panels show the residuals for line positions for the assigned lines versus the experimental positions.

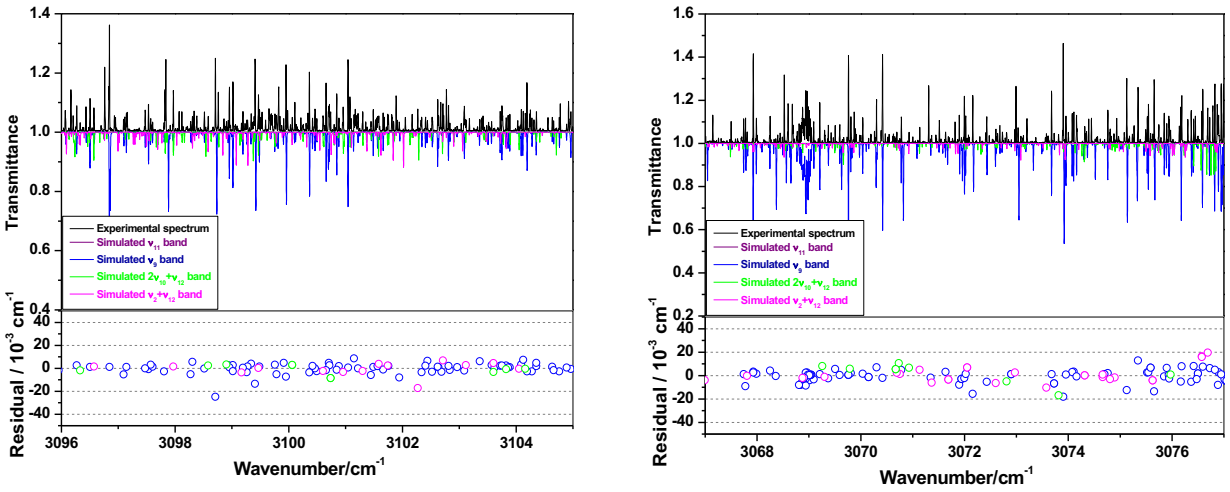

Fig. 5: Simulation of the region of the $\nu_2 + \nu_{12}$ and $2\nu_{10} + \nu_{12}$ bands. The lower panels show the residual Obs. – Calc. in cm^{-1} for line positions for the assigned lines versus the experimental positions.

The D_{2h}TDS package, from the XTDS software, was also used to calculate the rovibrational energy levels using the D_{2h}TDS package and fitted tensorial parameters listed above. This program can be used for any asymmetric top molecule with D_{2h} symmetry [32].

The reduced rovibrational energies of the ν_9, ν_{11}, $2\nu_{10} + \nu_{12}$ and $\nu_2 + \nu_{12}$ bands of ethylene are depicted in Fig. 6. All calculated energy levels are represented in this Figure by the blue points, whereas the magenta points depict the higher energy levels associated to the assigned transitions.

By definition, the reduced energies can be expressed as:

$$E_{reduced} = E(J, \tilde{C}) - \sum_{\Omega} t^{\Omega(0,0A_1)}_{\{GS\}\{GS\}} (J(J+1))^{\frac{\Omega}{2}}$$

$$= E(J, \tilde{C}) - t^{2(0,0A_1)} J(J+1) - t^{4(0,0A_1)} J^2(J+1)^2 - t^{6(0,0A_1)} J^3(J+1)^3, \qquad (12)$$

with, $t^{2(0,0A_1)}$, $t^{4(0,0A_1)}$ and $t^{6(0,0A_1)}$ are the second, fourth, sixth and eighth order scalar parameters of the Hamiltonian, respectively.

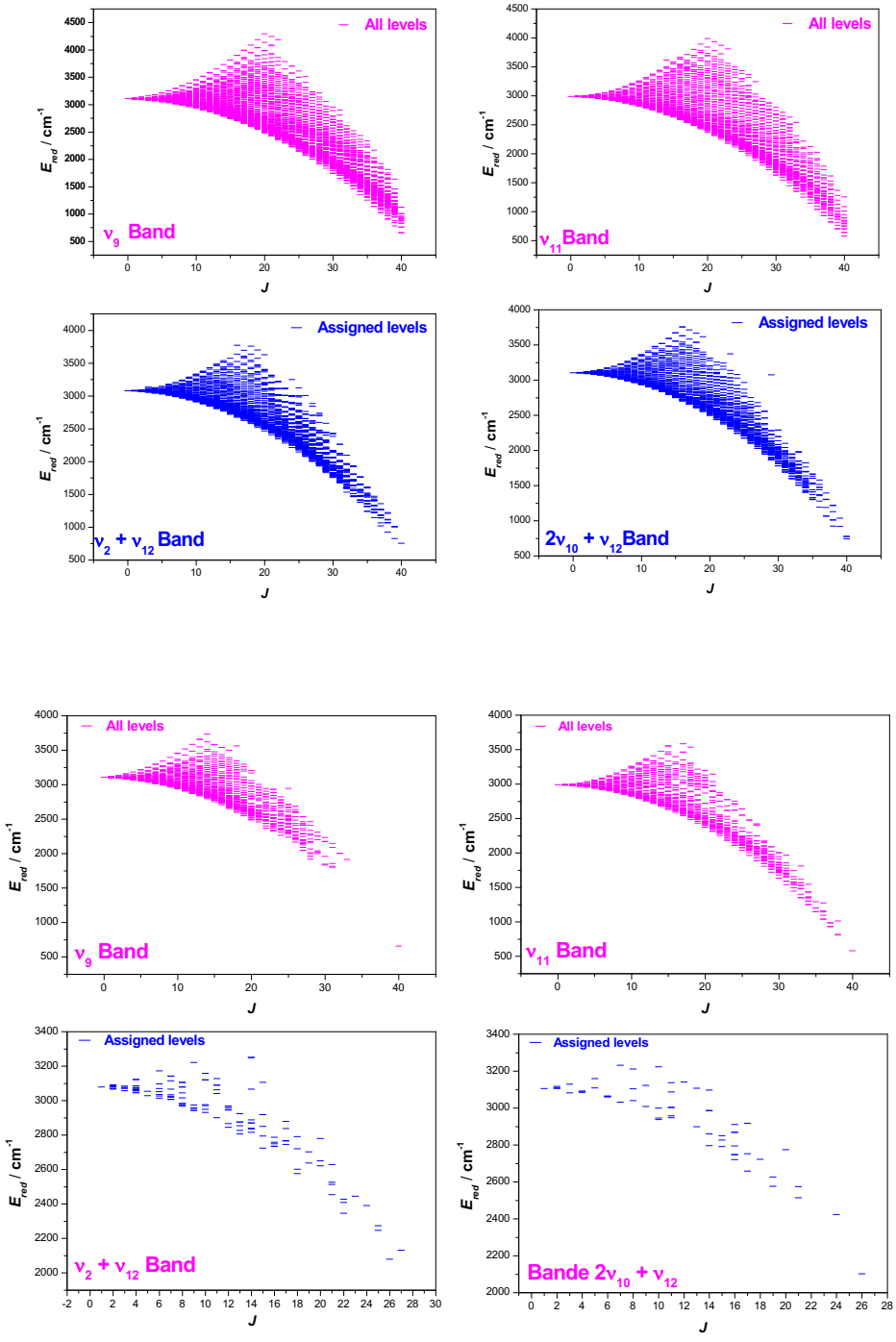

Fig. 6 : Energy levels of the ν_9, ν_{11}, $2\nu_{10}+\nu_{12}$ and $\nu_2+\nu_{12}$ bands of the 3000 cm^{-1} spectral region of the ethylene molecule, calculated using the D_{2h}TDS software.

The calculation of $E_{reduced}$ provides a clear and readable structure for large values of the quantum number J, as the energy levels cluster into packets with increasing J.

4.2. Correspondence between tensorial and Watson's parameters

In this sub-section, we will examine the comparison between the Watson's and the tensorial formalism in the ground and different excited vibrational states of the Polyad P_3. The tensorial rotational Hamiltonian, initially introduced by Moret-Bailly [45] for the study of spherical top molecules, can be written up to the sixth order as:

$$H_{Moret-Bailly} = t_1 \frac{\sqrt{3}}{4} R^{2(0,A_1)} + t_2 R^{2(2,E)} + t_3 R^{2(2,F_2)} + t_4 \frac{3}{16} R^{4(0,A_1)} + t_5 R^{4(2,E)} + t_6 R^{4(2,F_2)} + t_7 R^{4(4,A_1)} + t_8 R^{4(4,E)} + t_9 R^{4(4,F_2)} + t_{10} \frac{3\sqrt{3}}{64} R^{6(0,A_1)} + t_{11} R^{6(2,E)} + t_{12} R^{6(2,F_2)} + t_{13} R^{6(4,A_1)} + t_{14} R^{6(4,E)} + t_{15} R^{6(4,F_2)} + t_{16} R^{6(6,A_1)} + t_{17} R^{6(6,E)} + t_{18} R^{6(6,0F_2)} + t_{19} R^{6(6,1F_2)}. \quad (13)$$

In our work, we used the A-reduction of the Watson's Hamiltonian for the case of an asymmetric top molecule [46]:

$$H_{Watson}{}^{(A)} = \sum_\alpha B_\alpha^{(A)} J_\alpha{}^2 - \Delta_J (J^2)^2 - \Delta_{JK} J^2 J_z{}^2 - \Delta_K J_z{}^4 - \frac{1}{2}\left[\left(\delta_J J^2 + \delta_K J_z{}^2\right), \left(J_+^2 + J_-^2\right)\right]_+ + \Phi_J (J^2)^3 + \Phi_{JK} (J^2)^2 J_z{}^2 + \Phi_{KJ} J^2 J_z{}^4 + \Phi_K J_z{}^6 d_1 J^2 (J_+^2 + J_-^2) + \frac{1}{2}\left[\left(\varphi_J (J^2)^2 + \varphi_{JK} J^2 J_z{}^2 + \varphi_K J_z{}^4\right), \left(J_+^2 + J_-^2\right)\right]_+. \quad (14)$$

4.2.1. Corresponding formulas

The symbolic computation software Maple [47] was used to solve the equation $H_{Moret-Bailly} = H_{Watson}{}^{(A)}$ truncated at degree $\Omega = 6$ for the ethylene molecule. In order to convert the rotational constants into tensorial parameters, the employed formulas are given in Appendix. Note that a similar procedure using symbolic calculations was proposed by Rey *et al.* in the Appendix of [23] in order to derive at any order of the expansion a set of tensorial rotation-vibration parameters for molecules belonging to an arbitrary point group.

- For the I^r representation $B_x = C$, $B_y = B$, $B_z = A$.

The rotational constants in cm^{-1} in the Watson's model for the ground state (GS) of C_2H_4 are given in Table 3.

Table 3: Rotational constants in the Watson's model for the ground state (GS) of C_2H_4.

Constant	Value for the GS / cm^{-1}
A''	4.864554702
B''	1.000962032
C''	0.8280095375
Δ_J'' /10^{-06}	1.46574

Δ''_{JK} /10^{-05}	1.02256
Δ''_{K} /10^{-05}	8.64987
δ''_{J} /10^{-06}	-3.1823
δ''_{K} /10^{-05}	1.01443
Φ''_{J} /10^{-10}	6.76008
Φ''_{JK} /10^{-09}	-3.155876159
Φ''_{K} /10^{-09}	5.385698
Φ''_{KJ} /10^{-09}	2.124578
φ''_{J} /10^{-09}	1.0140
φ''_{JK} /10^{-09}	1.4460
φ''_{K} /10^{-09}	-2.2417454

Table 4: Rotational constants in cm^{-1} in the Watson's model for the v_9 =1, v_{11}= 1 and v_2 = v_{12} =1 levels of C_2H_4.

Constant	Value for v_{11}=1	Value for v_9=1	Value for $v_2 + v_{12}$=1
v'	2988.6435505	3104.8858750	3082.70272
$A' - A''$	-0.007343974810	-0.01829142477	0.02250811946
$B' - B''$	0.00005304053403	-0.002714908596	0.009991606416
$C' - C''$	-0.002463762178	- 0.001587706316	-0.006764788257
$(\Delta'_J - \Delta''_J)$ /10^{-05}	6.480208153	-1.263571269	3.378675688
$\Delta'_{JK} - \Delta''_{JK}$	-0.0002646118140	0.00005607703521	-0.0005863002044
$\Delta'_K - \Delta''_K$	0.0002295856868	0.00001478698953	0.001349734818
$(\delta'_J - \delta''_J)$ /10^{-05}	-1.248444509	-8.437203920	79.60261563
$\delta'_K - \delta''_K$	0.0001795513316	0.0002585292643	-0.002527223366
$(\Phi'_J - \Phi''_J)$ /10^{-6}	-4.340284696	2.915585324	- 9.476818425
$(\Phi'_{JK} - \Phi''_{JK})$ /10^{-06}	6.438921594	-4.510708878	12.47016725
$(\Phi'_K - \Phi''_K)$ /10^{-06}	1. 068435025	0.004866377150	5.144634231
$(\Phi'_{KJ} - \Phi''_{KJ})$ /10^{-06}	-3.144968485	1.844073303	-6.676508779
$(\varphi'_J - \varphi''_J)$ /10^{-06}	-6.659063763	3.762558768	-14.07257594
$(\varphi'_{JK} - \varphi''_{JK})$ /10^{-05}	1.006291401	-0.1764713202	1.886096991
$(\varphi'_K - \varphi''_K)$ /10^{-06}	-5.112835126	-1.354594431	-12.16738556

Table 5: Rotational constants in the Watson's model of the level $2v_{10} + v_{12}$ =1 of C_2H_4.

Constant	Value / cm^{-1}
$A' - A''$	0.02212787418
$B' - B''$	-0.003392590049
$C' - C''$	0.00757183317
$(\Delta'_J - \Delta''_J)$ /10^{-05}	-2.517488154
$(\Delta'_{JK} - \Delta''_{JK})$ /10^{-07}	5.542305438
$(\Delta'_K - \Delta''_K)$ /10^{-15}	-6.25
$(\delta'_J - \delta''_J)$ /10^{-08}	5.073056875
$(\delta'_K - \delta''_K)$ /10^{-15}	3.125
$(\Phi'_J - \Phi''_J)$ /10^{-15}	1.25

4.2.2. Conversion of the Fermi parameters

We first started from the Hamiltonian model of an asymmetric top molecule described in [14].

This model involves the transformation of one of the three rotational components J_α (α = *x, y, z*) according to the irreducible representation of type g in the D_{2h} group. Consequently, only vibrational states with symmetry Γ_g or with symmetry Γ_u interact with each other through the Hamiltonian:

$$H^{vib-rot} = \sum_{v,\tilde{v}} |v\rangle\langle\tilde{v}| H^{v\tilde{v}}. \quad (15)$$

The operators $H^{v\tilde{v}}$, which connect the vibrational states $|v\Gamma_g\rangle$ and $|\tilde{v}\Gamma_g\rangle$ with the same symmetry Γ_g, are the Fermi- type operators of the following form:

$$H_{v\tilde{v}} = {}^{v\tilde{v}}F_0 + {}^{v\tilde{v}}F_K J_z^2 + {}^{v\tilde{v}}F_J J^2 + {}^{v\tilde{v}}F_{KK} J_z^4 + {}^{v\tilde{v}}F_{KJ} J_z^2 J^2 + {}^{v\tilde{v}}F_{JJ} J^4 + \cdots + {}^{v\tilde{v}}F_{xy}\left(J_x^2 - J_y^2\right) + {}^{v\tilde{v}}F_{Kxy}\left[J_z^2\left(J_x^2 - J_y^2\right)\right] + {}^{v\tilde{v}}F_{Jxy} J^2\left(J_x^2 - J_y^2\right) + \cdots. \quad (16)$$

In our study, we examine Fermi interactions between the ν_{10}=2,ν_{12}=1 and ν_2=ν_{12}=1 levels, both exhibiting B_{1u} symmetry.

The first term in Eq. (16), ${}^{v\tilde{v}}F_0$ corresponds to the pure vibrational interaction, whereas the remaining terms describe the rotation-vibration components of the Fermi interaction. The ${}^{v\tilde{v}}F$ parameters associated with these interactions are compiled in Table 6. To determine these parameters, we used the equations in Appendix for the conversion from the tensorial parameters to Watson's ones.

Table 6: Fermi interaction parameters (in cm^{-1}) between the $|2\nu_{10} + \nu_{12}\rangle$ and $|\nu_2 + \nu_{12}\rangle$ states of C_2H_4.

Constant	Value / cm^{-1}
${}^{v\tilde{v}}F_0$	9. 594995
${}^{v\tilde{v}}F_K$	-0.00283889
${}^{v\tilde{v}}F_J$	0.0133104

4.2.3. Coriolis interaction

Coriolis-type interactions are present in the expression of the Hamiltonian through three distinct operators, where the main components proportional to (iJ_x, iJ_y et iJ_z) transform according to the irreducible representations B_{2g}, B_{1g} and B_{3g} of the D_{2h} group, respectively.

In our case, $|v\Gamma_g\rangle \otimes |v\tilde{\Gamma}_g\rangle = B_{2g}$, thus the interaction operator can be written as:

$$H_{v\tilde{v}} = iJ_x H_{v\tilde{v}}^{(1)} + H_{v\tilde{v}}^{(1)} iJ_x + \left[iJ_y, J_z\right]_+ H_{v\tilde{v}}^{(2)} + H_{v\tilde{v}}^{(2)}\left[iJ_y, J_z\right] + \left[iJ_x, \left(J_x^2 - J_y^2\right)\right]_+ H_{v\tilde{v}}^{(3)} +$$

$$H_{v\tilde{v}}^{(3)}\left[iJ_x,\left(J_x^2-J_y^2\right)\right]_+ +\cdots. \quad (17)$$

The operators $H_{v\tilde{v}}^{(i)}$ can be expressed in the following general form:

$$H_{v\tilde{v}}^{(i)} = \frac{1}{2}{}^{v\tilde{v}}C^i + {}^{v\tilde{v}}C_K^i J_z^2 + \frac{1}{2}{}^{v\tilde{v}}C_J^i J^2 + {}^{v\tilde{v}}C_{KK}^i J_z^4 + {}^{v\tilde{v}}C_{KJ}^i J_z^2 J^2 + \frac{1}{2}{}^{v\tilde{v}}C_{KJ}^i J^4. \quad (18)$$

In our work, we have considered interactions up to the first order. For the interaction $\langle v_9 \,|\, v_{11}\rangle$, we have determined the first-order parameter $C^1 = 0.0330127$ cm^{-1}. Additionally, for the interaction $v_9/2v_{10}+v_{12}$, we have determined six tensorial parameters, leading to the determination of further Watson's parameters. Particularly, we found $C^1 = -0.01799758$ cm^{-1}, $C_K^1 = -0.00251833$ cm^{-1} and $C_J^1 = 0.0050701$ cm^{-1}.

4.3. Intensity analyses

4.3.1. Line intensities

In this study, we used a non-linear least squares method to adjust the experimental line intensities, using our fitted Hamiltonian parameters to compute the line positions.

Figs. 7 and 8 illustrate the variations of the calculated and experimental intensities, as well as the differences between the observed and calculated values (Obs. – Calc.) in %, as a function of wavenumbers for the two fundamental bands ν_9 and ν_{11} as well as for the two combination bands $\nu_2+\nu_{12}$ and $2\nu_{10}+\nu_{12}$. No significant dispersions effects are observed, with deviations ranging from 1% to 10%.

Our analysis involved a total of 2190 assigned lines, distributed as follows: 1284 assignments in the ν_9 band, 851 in the ν_{11} band, 28 in the $\nu_2 + \nu_{12}$ and 27 in $2\nu_{10}+\nu_{12}$. These assignments were made by adjusting 14 parameters out of 23, including the vibrational dipole moments associated to each of the four bands.

Due to the limited number of assigned lines for the two combination bands, we could note that the corresponding vibrational dipole moments are not precisely determined. As a result, the estimation of line intensities and derived band intensities using Eqs. (20, 21) is not as accurate as that of line positions.

The tensor parameters obtained by fitting experimental intensities are presented in Table 7. The dipole moment operator was developed to the second order in this analysis. The overall Root-Mean-Square (RMS) deviation is about 3.77%.

In a previous study referenced as [19], the authors determined the dipole moment

parameters for the two fundamental bands. Their values are higher than ours, showing a difference of 10% for ν_9 and 20% for the ν_{11} band.

Table 7: Statistics of the intensity fitting for the 3.3 µm spectral region of the ethylene molecule.

Development Order of dipole moment	2
Assignments	2216
Fitted parameters	14/23
J_{max}	36
RMS (%)	3.77
Standard Deviation (SD)	3.13

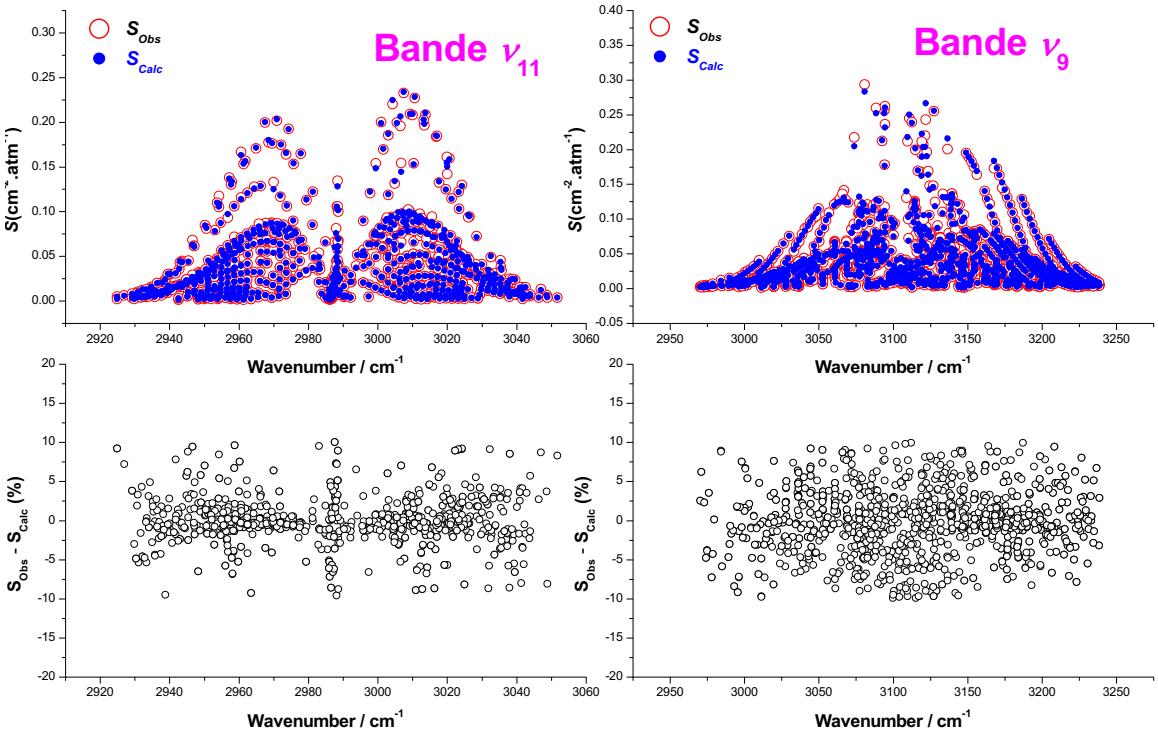

Fig. 7: Upper panels: observed and simulated line intensities of ethylene for the two fundamental bands ν_9 and ν_{11} as a function of the wavenumber. Lower panels: variation of their differences (Obs - Calc) in % as a function of the wavenumber.

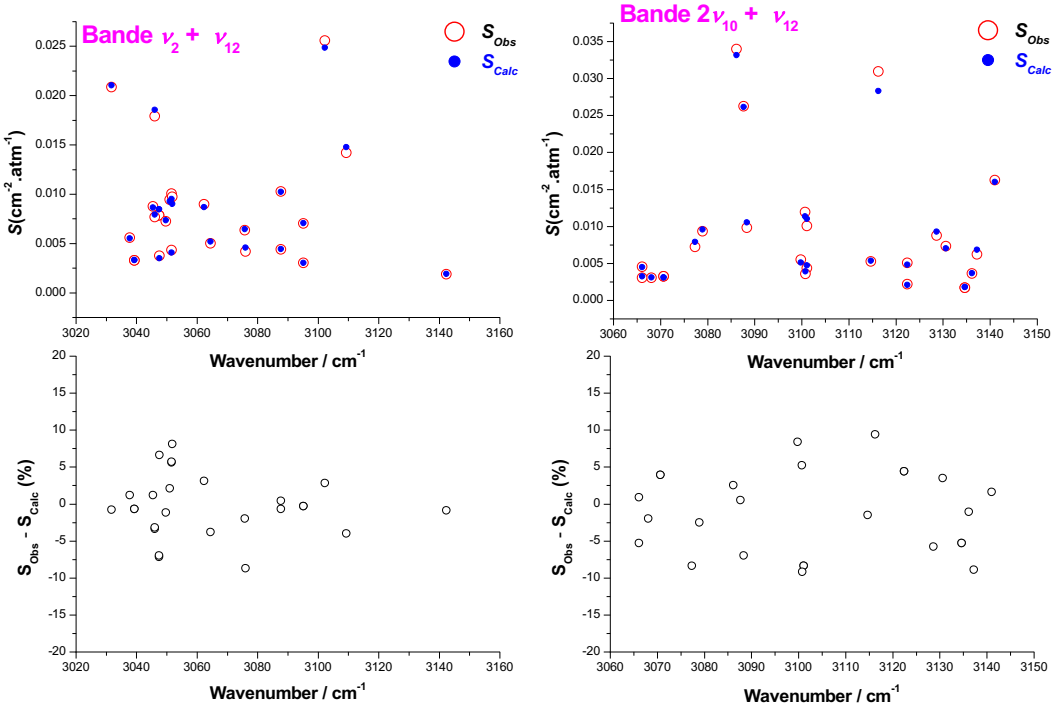

Fig. 8: Upper panels: observed and simulated line intensities of ethylene for the two combination bands $\nu_2 + \nu_{12}$ and $2\nu_{10}+\nu_{12}$ as a function of the wavenumber. Lower panels: variation of their differences (Obs - Calc) in % as a function of the wavenumber

Table 8: Effective dipole moment parameters in D (Debye) for the ν_9, ν_{11}, $\nu_2 + \nu_{12}$ and $2\nu_{10} + \nu_{12}$ bands of C_2H_4.

Band	***Order***	***Vibrational states***			***Value / D***
		Ω(K,nΓ)	Γ_v	Γ'_v	
$\boldsymbol{\nu_9}$	0	$0(0,0A_g)$	$000000000000A_g$	$000000001000B_{3u}$	3. 06987(63) $\times 10^{-02}$
	1	$1(1,0B_{1g})$	$000000000000A_g$	$000000001000B_{3u}$	1. 7474(29) $\times 10^{-04}$
		$1(1,0B_{2g})$	$000000000000A_g$	$000000001000B_{3u}$	9.79(22) $\times 10^{-06}$
	2	$2(0,0A_g)$	$000000000000A_g$	$000000001000B_{3u}$	1.76(13) $\times 10^{-07}$
		$2(2,0A_g)$	$000000000000A_g$	$000000001000B_{3u}$	3.78(18) $\times 10^{-07}$
		$2(2,1A_g)$	$000000000000A_g$	$000000001000B_{3u}$	0.0
		$2(2,0B_{1g})$	$000000000000A_g$	$000000001000B_{3u}$	0.0
		$2(2,0B_{2g})$	$000000000000A_g$	$000000001000B_{3u}$	0.0
$\boldsymbol{\nu_{11}}$	0	$0(0,0A_g)$	$000000000000A_g$	$000000000010B_{1u}$	2.39051(61) $\times 10^{-02}$
	1	$1(1,0B_{2g})$	$000000000000A_g$	$000000000010B_{1u}$	1.60(34) $\times 10^{-06}$
		$1(1,0B_{3g})$	$000000000000A_g$	$000000000010B_{1u}$	-1.890(41) $\times 10^{-05}$
	2	$2(0,0A_g)$	$000000000000A_g$	$000000000010B_{1u}$	-5.44(26) $\times 10^{-07}$
		$2(2,0A_g)$	$000000000000A_g$	$000000000010B_{1u}$	9.03(36) $\times 10^{-07}$
		$2(2,1A_g)$	$000000000000A_g$	$000000000010B_{1u}$	0.0
		$2(2,0B_{2g})$	$000000000000A_g$	$000000000010B_{1u}$	0.0
		$2(2,0B_{3g})$	$000000000000A_g$	$000000000010B_{1u}$	0.0
$\boldsymbol{\nu_2 + \nu_{12}}$	0	$0(0,0A_g)$	$000000000000A_g$	$010000000001B_{1u}$	1.0314(21) $\times 10^{-02}$
	1	$1(1,0B_{2g})$	$000000000000A_g$	$010000000001B_{1u}$	9 (1) $\times 10^{-06}$
		$1(1,0B_{3g})$	$000000000000A_g$	$010000000001B_{1u}$	5.68(11) $\times 10^{-05}$
$\boldsymbol{2\nu_{10} + \nu_{12}}$	0	$0(0,0A_g)$	$000000000000A_g$	$000000000201B_{1u}$	5.553(16) $\times 10^{-03}$

If we look now at the spectrum structure, we can note that certain pairs of lines such as

(A_g,B_{1g}), (A_g,B_{2g}) and (A_g,B_{3g}) exhibit different symmetries, are sometimes resolved and sometimes not resolved as shown in Fig. 9.

Due to the ½ spin of the H ligands, the C_2H_4 have spin statistical weights ω_i for each D_2 symmetry species A, B_1, B_2 or B_3. These weights are 7, 3, 3 and 3, respectively. Thus, for a cluster of n = 2 or 3 lines with experimental total intensity I_{Exp}, the intensity of the "subline" i can be extracted as:

$$I_{Exp}^{i} = \frac{\omega_i \, I_{Exp}^{i}}{\sum_{j=1}^{n} \omega_j} \tag{19}$$

The upper panel corresponds to transitions from the Q branch of the ν_9 band, where the lines of symmetries A_g and B_{1g} coincide at the same frequency. In contrast, the lower panel exhibits an example of two lines from the R branch of the ν_9 band that are well resolved with clearly different intensities. The intensity differences of these pairs of lines are due to the fact that these two symmetries have different spin statistical weights (7 for the A_g symmetry and 3 for B_{1g}).

Likewise, for the pairs of lines featuring symmetries such as (B_{1g}, B_{2g}), (B_{1g}, B_{3g}), (B_{2g}, B_{3g}), as shown in Fig. 10, transitions with symmetries B_{2g} and B_{3g} from the Q branch of the ν_9 band are coincident.

The lower panel displays a resolved doublet of lines in the P branch of the ν_{11} band; the B_{1g} *and* B_{3g} components of this doublet have identical intensities. This uniformity of line intensities can be attributed to the equal spin statistical weight of the B_{1g}, B_{2g} and B_{3g} symmetries, each having a weight of 3.

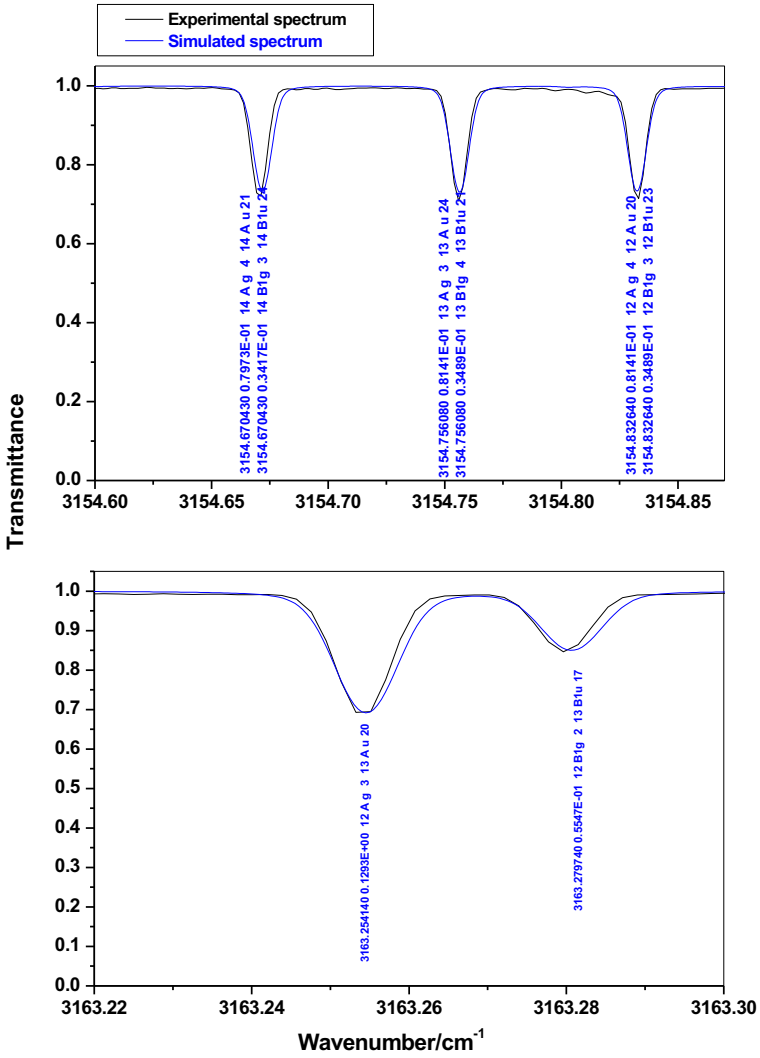

Fig. 9: The upper panel illustrates a detailed experimental and simulated spectrum of C_2H_4, showing the coincidence of the Q branch transitions from the ν_9 band with symmetries (A_g and B_{1g}). The lower panel shows a pair of resolved lines from the same band, characterized by identical symmetries (A_g and B_{1g}). The labels express respectively, the experimental position, the experimental intensity, J'', symmetry of the lower level, the multiplicity index n on a level patch having the same J associated to the lower level, J', symmetry of the upper level and the multiplicity index n associated to the upper level.

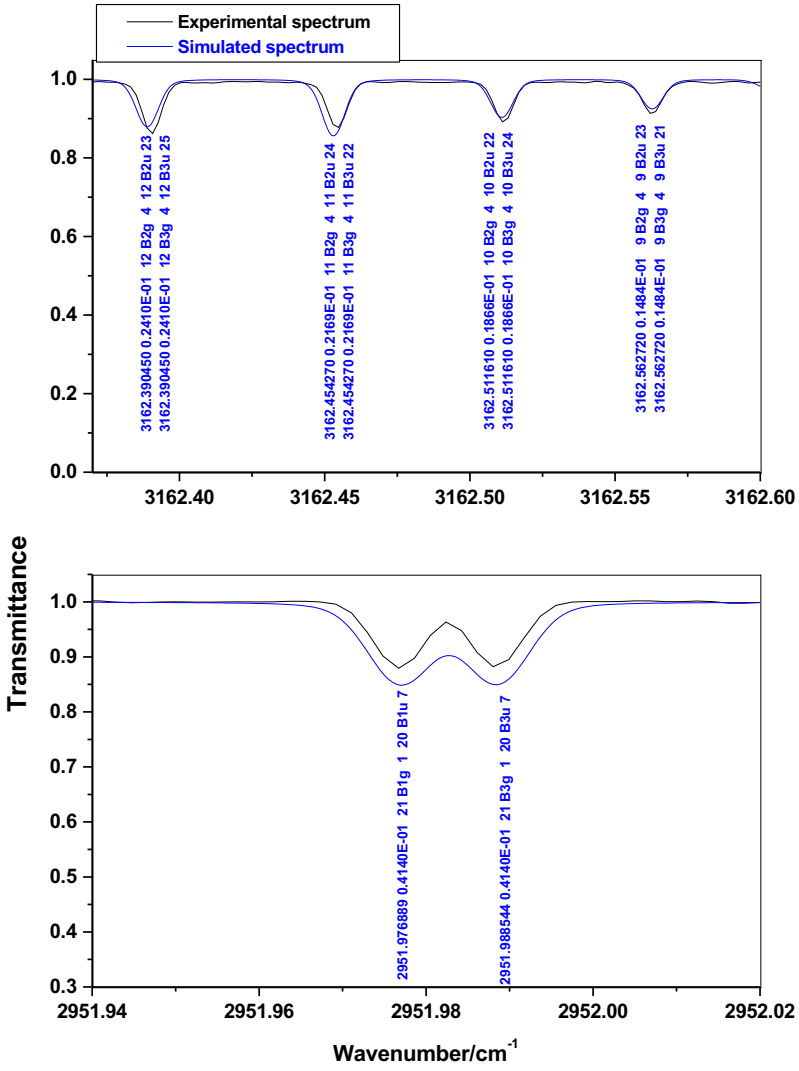

Fig. 10: The upper panel illustrates a detailed part of the experimental and simulated transmission spectrum of C_2H_4 showing the coincidence of some transitions of the ν_9 band having the same symmetries (B_{2g} and B_{3g}). The lower panel shows a resolved doublet of the ν_{11} band also with the same symmetries (B_{1g} and B_{3g}). The labels express respectively, the experimental position, the experimental intensity, J'', symmetry of the lower level, the multiplicity index n on a level patch having the same J associated to the lower level, J', symmetry of the upper level and the multiplicity index n associated to the upper level.

4.3.2. Band intensity

The vibrational transition dipole moments for each band are provided in Table 9. These moments correspond to the zeroth-order tensor parameter $(0,0,0A_g)$ in the dipole moment expansion. The band intensities S_v can be calculated as:

$$S_v = \frac{8\pi^3 \sigma_v N_0 T_0}{3hcQ_{vib}T} \exp\left(-\frac{E_v}{kT}\right) \mu_v^2 . \qquad (20)$$

Alternatively, we can determine the intensity of each band using the summation method

with the following approximate relationship:

$$S^{(s)}{}_{v} \approx \sum_{k} S_k \,. \tag{21}$$

The intensity S_k corresponds to each line k, and the summation extends over all lines in the list. The results obtained from both methods are presented in Table 10, along with a comparison with literature data determined using the summation method [48, 49], the method with Eq. (20) [22], and the band surface method through the Beer-Lambert law [50]. According the *ab initio* calculated line lists in [11], the contribution of the ν_9, ν_{11}, $\nu_2 + \nu_{12}$ and $2\nu_{10} + \nu_{12}$ represents ~97% of the total intensity of the 3-micron region. In this reference, calculations based on an effective model were performed in the spectral region of 3000 cm^{-1}. The authors determined the intensities of 24 bands, of which 4 are presented in Table 9. Additionally, the sum of the other 20 bands accounts for only 3% of the total intensity in this region. Despite their low intensity contributions, they have the potential to resonate with the four prominent bands, leading to perturbations in their positions.

A good agreement of 1 and 9% for the ν_9 and ν_{11}, respectively is found with this reference.

By comparing our results using both methods, it can be observed that the first method yields consistent results for determining the intensities of combination bands. As expected, the intensity of the 2-quanta $\nu_2 + \nu_{12}$ band is higher than that of the 3-quanta $2\nu_{10} + \nu_{12}$ band.

It is noteworthy that the sum intensity of these two bands is almost equal using both methods.

Additionally, the determination of the transition moments of these bands and their corresponding intensities are affected by strong band interactions in this spectral region, leading to an intensity transfer between bands in the studied spectral region.

Comparing our band intensities values with HITRAN 2020 [48], the average differences are 4%, 4%, 21%, and 7% for the ν_9, ν_{11}, $\nu_2 + \nu_{12}$, and $2\nu_{10} + \nu_{12}$ bands, respectively. It should be noted that a difference of 14% is found when comparing the sum of the intensities of the ν_9 and $\nu_2 + \nu_{12}$ bands with Ref. [49]. For the ν_9 band, differences of 5% and 13% are observed when it was compared to Refs. [22, 50], respectively.

Regarding the ν_{11} band, the deviations between our results and Refs. [49, 50 and 22] are around 9%, 10% and 23%, respectively.

Table 9: Band intensity of ν_9, ν_{11}, $\nu_2 + \nu_{12}$ and $2\nu_{10} + \nu_{12}$ bands and comparison with literature data. S_v et $S_v^{(s)}$ are given respectively by the eqs. (20) and (21).

Band	S_v **/ (cm^{-2}/atm)**	$S_v^{(s)}$ **/ (cm^{-2}/atm)**

	Present work	**Ref.** [22]	**Present work**	**Ref.** [48]	**Ref.** [49]	**Ref.** [50]	**Ref.** [11]
$\boldsymbol{\nu_9}$	86.52(33)	82.52(86)	84.58	82.75	112.20(24)	100(3)	83.6
$\boldsymbol{\nu_2 + \nu_{12}}$	9.69(7)		5.70	7.64			8.85
$\boldsymbol{\nu_{11}}$	50.50(20)	65.87(64)	50.15	48.57	55.35(14)	56.0(3)	52.7
$\boldsymbol{2\nu_{10} + \nu_{12}}$	2.83(3)		6.40	3.05			7.76

Table 10 displays a comparison between our integrated intensity values (in cm/molecule) in the spectral region between 2900 and 3300 cm^{-1} with those of Refs. [11, 52]. The observed differences are 10% and 6%, respectively.

Table 10: Comparison of our calculation of integrated intensities (PW) with those of the empirical calculation of HITRAN [52], the experimental databases of the PNNL [51] and Ref. [11].

Spectral region/ cm^{-1}	**Integrated intensity/ cm. molecule^{-1} $\times 10^{-18}$**		
	Ref. [11]	PNNL [51]	HITRAN 2020 [48]
2900 - 3300	6.64	6.86	5.64

5. ECaSDa database update

We have updated the ECaSDa database by using a new polyad scheme adapted to this work. The first scheme that was defined previously is dedicated to the $\nu_{10}/\nu_7/\nu_4/\nu_{12}$ band system, at 10 μm region, while the second and new one corresponds to the present analysis. We also raised the threshold value to 10^{-27} cm^{-1}/(molecule cm^{-2}), significantly reducing the number of lines of scheme 1 included in our computation. The complete database, illustrated in Table 12, contains a total of 96 397 lines, and is accessible through our website at https://vamdc/icb.cnrs.fr/PHP/ecasda.php. Our web page allows data to be plotted and retrieved in two formats. Line by line is downloadable in HITRAN 2004 format, while cross section that are computed by the binned sum of intensities is just a simple 2-column flat file. However, it is important to mention that the HITRAN file produced by our database is different from the one available on the HITRAN online website, in order to conform to our formalism and fully describe the vibrational states [53].

Table 12: Rovibrational transitions in ECaSDa. The polyad schemes are described by the (i_1; i_2; …; i_N) satisfying the relation $= \sum_{k=1}^{k=N} i_k \nu_k$, where N is the polyad number.

Transitions	Nb. dipolar	Dipolar wavenumber / cm^{-1}	Dipolar intensity / cm^{-1}/(molecule cm^{-2})
$^{12}C_2H_4$			

Scheme 1 (0,0,0,1,0,0,1,0,0,1,0,1)			
$P_1 - P_0$	54 755	650 – 1525	$10^{-27} – 10^{-20}$
Scheme 2 (0,2,0,0,0,0,0,0,3,1,3,1)			
$P_3 - P_0$	41 642	2900 – 3300	$10^{-27} – 10^{-19}$
Total	96 397		

6. Conclusion

In this paper, we have reported the line position and line intensity analyses of the ν_9, ν_{11}, 2 ν_{10}+ ν_{12} and ν_2+ ν_{12} interacting band system of the ethylene molecule in the spectral range from 2900 to 3300 cm^{-1}. To this end, we used the D_{2h}TDS software to analyze this complex band system.

In total, we assigned 3328 lines and fitted 88 Hamiltonian parameters, including ten Coriolis interaction parameters and four Fermi parameters, with an RMS precision of 5.927 × 10^{-3} cm^{-1}.

We have also converted these parameters to the Watson's ones, especially for the $2\nu_{10}+\nu_{12}$ band that are absent in the literature, by using the correspondence formulas between the tensorial and the Watson formalism given in Appendix.

In the last part, we presented the results of line intensity adjustment. We managed to fit fourteen transition moment parameters with an RMS accuracy of 3.77%. We then calculated the cross sections of the studied spectral region and compared them with data from the literature.

In order to go further in the understanding of both weak and strong spectral features and in the modelling of the overall 3.3 μm region, accounting for all dark states in strong resonance with the "bright" states will be required. Undoubtedly, the method presented in [23] based on the construction of non-empirical effective models by avoiding van Vleck-type perturbation theory could be of great help in the determination of a first set Hamiltonian and dipole moment parameters to be slightly refined on observation.

References

[1] Sawada S, Totsuka T. Natural and anthropogenic sources and fate of atmospheric ethylene. Atmos Environ 1986;20:821-32. https://doi.org/10.1016/0004-6981(86)90266-0.

[2] Seifert R, Delling N, Richnow HH, Kempe S, Hefter J, Michaelis W. Ethylene and methane in the upper water column of the subtropical Atlantic. Biogeochemistry 1999;44:73-91.

[3] Herbin H, Hurtmans D, Clarisse L, Turquety S, Clerbaux C, Rinsland CP, Boone C, Bernath PF, Coheur PF. Distributions and seasonal variations of tropospheric ethene (C_2H_4) from Atmospheric Chemistry Experiment (ACE-FTS) solar occultation spectra. Geophys Res Lett 2009;36:L04801. https://doi.org/10.1029/2008GL036338.

[4] Gentner DR, Worton DR, Isaacman G, Davis LC, Dallmann TR, Wood EC, Herndon SC, Goldstein AH, Harley RA. Chemical composition of gas-phase organic carbon emissions from motor vehicles and implications for ozone production. Environ Sci Technol 2013;47:11837-48. https://doi.org/10.1021/es401470e.

[5] Romani PN, Jennings DE, Bjoraker GL, Sada PV, McCabe GH, Boyle RJ. Temporally varying ethylene emission on Jupiter. Icarus 2008;198:420-34. https://doi.org/10.1016/j.icarus.2008.05.027.

[6] Hesman BE, Bjoraker GL, Sada PV, Achterberg RK, Jennings DE, Romani PN, Lunsford AW, Fletcher LN, Boyle RJ, Simon-Miller AA, Nixon CA, Irwin PGJ. Elusive ethylene detected in Saturn's northern storm region. Astrophys J 2012;760:24. https://doi.org/10.1088/0004-637X/760/1/24.

[7] Coustenis A, Jennings DE, Nixon CA, Achterberg RK, Lavvas P, Vinatier S, Teanby NA, Bjoraker GL, Carlson RC, Piani L, Bampasidis G, Flasar FM, Romani PN. Titan trace gaseous composition from CIRS at the end of the Cassini-Huygens prime mission. Icarus 2010;207:461-76. https://doi.org/10.1016/j.icarus.2009.11.027

[8] Encrenaz T. ISO observations of planetary atmospheres. Adv Space Res 2002;30:1967-70. https://doi.org/10.1016/S0273-1177(02)00565-3.

[9] Vander Auwera J, Fayt A, Tudorie M, Rotger M, Boudon V, Franco B, Mahieu E. Self-broadening coefficients and improved line intensities for the ν_7 band of ethylene near 10.5 μm, and impact on ethylene retrievals from Jungfraujoch solar spectra. J Quant Spectrosc Radiat Transf 2014;148:177-85. https://doi.org/10.1016/j.jqsrt.2014.07.003.

[10] Georges R, Bach M, Herman M. The vibrational energy pattern in ethylene ($^{12}C_2H_4$). Mol Phys 1999;97:279-92. https://doi.org/10.1080/00268979909482829.

[11] Rey M, Delahaye T, Nikitin AV, Tyuterev VG, First theoretical global line list of ethylene ($^{12}C_2H_4$) spectra for the temperature range 50-700 K in the far-infrared for quantification of absorption and emission in planetary atmospheres, A&A 2016;597:A47. https://doi.org/10.1051/0004-6361/201629004.

[12] Ulenikov ON, Gromova OV, Aslapovskaya Yu. S, Horneman V-M. High resolution spectroscopic study of C_2H_4: Re-analysis of the ground state and ν_4, ν_7, ν_{10}, and ν_{12} vibrational bands**.** J Quant Spectrosc Radiat Transf 2013;118:14–25. https://doi.org/10.1016/j.jqsrt.2012.11.032.

[13] Ulenikov O.N, Gromova O.V, Bekhtereva E.S, Aslapovskaya Yu. S, Tan T.L, Sydow C, Maul C, Bauerecker S. Ethylene-1-$^{13}C(^{13}C^{12}CH_4)$: First analysis of the ν_2, ν_3 and $2\nu_{10}$ bands and re–analysis of the ν_{12} band and of the ground vibrational state. J Quant Spectrosc Radiat Transf 2017;187: 403–13. https://doi.org/10.1016/j.jqsrt.2016.10.009.

[14] Ulenikov ON, Gromova OV, Bekhtereva ES, Onopenko GA, Aslapovskaya Yu. S, Gericke K-H, Bauerecker S, Horneman V-M. High resolution FTIR study of the $\nu_7+\nu_{10}-\nu_{10}$ and $\nu_{10}+\nu_{12}-\nu_{10}$ "hot" bands of C_2H_4. J Quant Spectrosc Radiat Transf 2014;149:318-33. https://doi.org/10.1016/j.jqsrt.2014.08.013.

[15] Ulenikov ON, Gromova OV, Bekhtereva ES, Kashirina NV, Onopenko GA, Maul C, Bauerecker S. Ro-vibrational analysis of the hot bands of $^{13}C_2H_4$: $\nu_7+\nu_{10}-\nu_{10}$ and $\nu_{10}+\nu_{12}-\nu_{10}$. J Mol Spectrosc 2015;317: 32–40. https://doi.org/10.1016/j.jms.2015.08.010.

[16] Ben Hassen A, Galalou S, Kwabia Tchana F, Dhib M, Aroui H. Self- and N_2-collisional broadening coefficients of ethylene in the 1800-2350 cm^{-1} spectral region. J Quant Spectrosc Radiat Transf 2016;326:73-80. https://doi.org/10.1016/j.jms.2016.03.013.

[17] Hurtmans D, Rizopoulos A, Herman M, Hassan LMS, Perrin A. Vibration-rotation analysis of the jet-cooled ν_{12}, $\nu_7+\nu_8$ and $\nu_6+\nu_{10}$ absorption bands of $^{12}C_2H_4$. Mol Phys 2001;99:455-61.

https://doi.org/10.1080/00268970010017018.
[18] Oomens J, Reuss J, Mellau GC, Klee S, Gulaczyk I, Fayt A. The ethylene hot band spectrum near 3000 cm^{-1}. J Mol Spectrosc 1996;180:236-48. https://doi.org/10.1006/jmsp.1996.0247.
[19] Sartakov BG, Oomens J, Reus J, Fayt A. Interaction of vibrational fundamental and combination states of ethylene in the 3 μm region. J Mol Spectrosc 1997;185:31-47. https://doi.org/10.1006/jmsp.1997.7378.
[20] Bach M, Georges R, Hepp M, Herman M. Slit-jet transform infrared spectroscopy in $^{12}C_2H_4$: cold and hot bands near 3000 cm^{-1}. Chem Phys Lett 1998;294:533-7. https://doi.org/10.1016/S0009-2614(98)00889-6.
[21] Lorono Gonzalez MA, Boudon V, Loëte M, Rotger M, Bourgeois MT, Didriche K, Herman M, Kapitanov VA, Ponomarev YN, Solodov AA, Solodov AM, Petrova TM. High-resolution spectroscopy and preliminary global analysis of C–H stretching vibrations of C_2H_4 in the 3000 and 6000 cm^{-1} regions. J Quant Spectrosc Radiat Transf 2010;111:2265-78. https://doi.org/10.1016/j.jqsrt.2010.04.010.
[22] Dang-Nhu M, Pine AS, Fayt A, De Vleeschouwer M, Lambeau C. Les intensités dans la pentade ν_{11}, $\nu_2+\nu_{12}$, $2\nu_{10}+\nu_{12}$ et $\nu_3+\nu_8+\nu_{10}$ de $^{12}C_2H_4$. Can J Phys 1983;61:514-21. https://doi.org/10.1139/p83-065.
[23] Rey M. Novel methodology for systematically constructing global effective models from ab initio-based surfaces: A new insight into high resolution molecular spectra analysis. J Chem Phys 2022;156:224103. https://doi.org/10.1063/5.0089097.
[24] Carleer M.R, in Remote Sensing of Clouds and the Atmosphere V, edited by J.E. Russel, K. Schäfer, and O. Lado Bordowsky, Vol. 4168 (Proceedings of SPIE – the International Society for Optical Engineering, Barcelona, Spain, 2001), p. 337. https://doi.org/10.1117/12.413851.
[25] Rothman LS et al., The HITRAN 2008 molecular spectroscopic database, J Quant Spectrosc Radiat Transf 2009;110:533-72. https://doi.org/10.1016/j.jqsrt.2009.02.013.
[26] Toth RA, Linelist of water vapor parameters from 500 to 8000 cm^{-1} (unpublished), https://mark4sun.jpl.nasa.gov/h2o.html.
[27] Farji A, Aroui H, Vander Auwera J, Air-induced collisional parameters in the ν_3 band of methane, J Quant Spectrosc Radiat Transf 2021;275:107878. https://doi.org/10.1016/j.jqsrt.2021.107878.
[28] Rotger M, Boudon V, Vander Auwera J, Line positions and intensities in the ν_{12} band of ethylene near 1450 cm^{-1}: An experimental and theoretical study, J Quant Spectrosc Radiat Transf 2008;109:952-62. https://doi.org/10.1016/j.jqsrt.2007.12.005.
[29] Wenger Ch, Boudon V, Champion J-P, Pierre G. Highly-spherical Top Data System (HTDS) software for spectrum simulation of octahedral XY_6 molecules. J Quant Spectrosc Radiat Transf 2000;66:1-16. https://doi.org/10.1016/S0022-4073(99)00161-2.
[30] Champion JP, Loëte M, Pierre G. In: Narahari Rao K, Weber A, editors. Spectroscopy of the Earth's atmosphere and interstellar medium. San Diego: Academic Press; 1992. p. 339–422.
[31] Cheblal N, Boudon V, Loëte M. Development of the dipole moment and polarizability operators of octahedral molecules. J. Mol. Spectrosc. 1999;197:222–31. https://doi.org/10.1006/jmsp.1999.7902.
[32] Wenger Ch, Rotger M and Boudon V. D_{2h} top data system (D_{2h}TDS) software for spectrum simulation of X_2Y_4 asymmetric molecules. J Quant Spectrosc Radiat Transf 2005;95: 521-538. https://doi.org/10.1016/j.jqsrt.2004.11.012.
[33] Boudon V, Champion J-P, Gabard T, Loëte M, Michelot F, Pierre G, Rotger M, Wenger Ch and Rey M. Symmetry-Adapted Tensorial Formalism to Model Rovibrational and Rovibronic Spectra of Molecules Pertaining to Various Point Groups. J Mol Spectrosc 2004;228:620–34. https://doi.org/10.1016/j.jms.2004.02.022.
[34] Raballand W, Rotger M, Boudon V and Loëte M. Spectroscopy of X_2Y_4 (D_{2h}) molecules: tensorial formalism adapted to the $O_3 \supset D_{2h}$ chain, Hamiltonian and transition moment operators. J Mol Spectrosc 2003:35217:239–48. https://doi.org/10.1016/S0022-2852(02)00038-3.
[35] Herzberg G. Infrared and Raman spectra of polyatomic molecules. New York: D Van Nostrand Company Inc, 1945.

[36] Wilson E. B and Howard J. B. The Vibration Rotation Energy Levels of Polyatomic Molecules I. Mathematical Theory of Semi-rigid Asymmetrical Top Molecules. J Chem Phys 1936;4:260. https://doi.org/10.1063/1.1749833.

[37] Wenger Ch , Boudon V, Rotger M, Sanzharov M, Champion J.-P. XTDS and SPVIEW: Graphical tools for the analysis and simulation of high-resolution molecular spectra. J Mol Spectrosc 2008;251:102-13. https://doi.org/10.1016/j.jms.2008.01.011.

[38] Lebron G.B, Tan T.L. High-resolution Fourier transform infrared spectrum of the ν_{11} band of ethylene ($^{12}C_2H_4$). J Mol Spectrosc 2013;288:11-13. https://doi.org/10.1016/j.jms.2013.03.008.

[39] https://icb.u-bourgogne.fr/spview/.

[40] Jan M. L. Martin. The anharmonic force field of ethylene, C_2H_4, by means of accurate *ab initio* calculations. J Chem Phys 1995;103:2589. https://doi.org/10.1063/1.469681.

[41] Duncan J.L, Hamilton E. An improved general harmonic force field for ethylene. J Mol Struct Theochem 1981;76:65-80. https://doi.org/10.1016/0166-1280(81)85114-7.

[42] Ballandras A, Cirtog M, Loroño M. A, Bourgeois M.-T, Rotger M, Bermejo D, Martínez R. Z, Doménech J. L and Boudon V. High-resolution stimulated Raman spectroscopy and analysis of the ν_2 and ν_3 bands of C_2H_4. J Raman Spectrosc 2013;44:1033-8. https://doi.org/10.1002/jrs.4328

[43] Loroño M, Bermejo D, Rotger M and Boudon V. High-resolution stimulated Raman spectroscopy and analysis of the $2\nu_{10}$ overtone symmetric motion of C_2H_4. J Raman Spectrosc 2009; 40:1065-71. https://doi.org/10.1002/jrs.2239.

[44] Lebron G. B and Tan T. L. High-resolution Fourier transform infrared spectrum of the ν_{12} band of ethylene ($^{12}C_2H_4$). Cosmos 2013;9:29-35. https://doi.org/10.1142/S0219607713500018.

[45] Moret-Bailly J. Interpretation of rotation-vibration spectra of molecules with tetrahedral or octahedral symmetry, Cahiers de Physique 1961;15:237.

[46] Papousek D, Aliev M.R. Molecular vibrational–rotational spectra. Elsevier, New York; 1982.

[47] http://www.maplesoft.com.

[48] Gordon IE *et al*. The HITRAN2020 molecular spectroscopic database. J Quant Spectrosc Radiat Transf 2022;277:107949. https://doi.org/10.1016/j.jqsrt.2021.107949.

[49] G. B. Lebron and T. L. Tan. Integrated Band Intensities of Ethylene ($^{12}C_2H_4$) by Fourier Transform Infrared Spectroscopy. Hindawi Publishing Corporation (2012) ID 474639.

[50] Golike R. C, Mills I. M, Person W. B and Bryce Crawford JR. Vibrational Intensities. VI. Ethylene and its Deutero-isotopes. J Chem Phys 1956; 25:1266. https://doi.org/10.1063/1.1743191.

[51] Johnson T. J, Sams R. L et Sharpe S. W. The PNNL Quantitative Infrared Database for Gas-Phase Sensing: A Spectral Library for Environmental, Hazmat and Public Safety Standoff Detection. Proc. SPIE − The Int. Soc. Opt. Eng. 2004; 5269, 159. https://doi.org/10.1117/12.515604.

[52] Rothman L.S. et al. The HITRAN 2012 molecular spectroscopic database. J Quant Spectrosc Radiat Transf 2013;130: 4-50. https://doi.org/10.1016/j.jqsrt.2015.12.012.

[53] Richard C, Boudon V, Rotger M. Calculated spectroscopic databases for the VAMDC portal: New molecules and improvements. J Quant Spectrosc Radiat Transf 2020;251:107096. https://doi.org/10.1016/j.jqsrt.2020.107096.